







A sequential drug delivery system based on silk fibroin scaffold for effective cartilage repair

Menglin Xiao^{a,b}, Liangyan Sun^{a,c} , Kang Wu^{a,b} , Yuqi Ding^{a,c}, Peipei Wang^{a,c},
Chuangchuang Mu^{a,c}, Jinrong Yao^{a,b}, Zhengzhong Shao^{a,b}, Bingjiao Zhao^{a,c,**} ,
Xin Chen^{a,b,*} 

^a Department of Macromolecular Science, Department of Orthodontics, Multidisciplinary Consultant Center, Shanghai Stomatological Hospital & School of Stomatology, Fudan University, Shanghai, 200433, China

^b State Key Laboratory of Molecular Engineering of Polymers, Laboratory of Advanced Materials, Fudan University, Shanghai, 200433, China

^c Shanghai Key Laboratory of Craniomaxillofacial Development and Diseases, Fudan University, Shanghai, 200001, China

ARTICLE INFO

Keywords:

Silk protein
Sequential drug release
Recruitment
Chondrogenesis
Cartilage repair

ABSTRACT

Endogenous repair of cartilage defects is a preferential strategy for cartilage repair, but always hindered by insufficient early-stage cells and incomplete cell differentiation at later stages. For *in-situ* cartilage regeneration, it is crucial to develop a sequential drug release system capable of recruiting endogenous bone marrow mesenchymal stem cells (BMSCs) and promoting their chondrogenic differentiation. Herein, based on our long-term and fruitful research on silk fibroin (SF) porous scaffolds, a cell-free sequential drug delivery SF scaffold was developed. BMSCs affinity peptide PFSSTKT (PFS) was coated on the surface of SF scaffold, in which chondrogenic inducer kartogenin (KGN) and anti-inflammatory factor dexamethasone (DEX) were loaded. PFS was rapidly released within the first 10 days while KGN and DEX could be released over 28 days. The scaffold promoted BMSCs migration and chondrogenic differentiation through the release of PFS and KGN *in vitro*. Finally, the sequential drug released by the implanted SF scaffolds in rats indeed recruited endogenous BMSCs and significantly promoted the *in-situ* regeneration of their knee cartilage defects. In summary, this study not only introduces a green and environmentally friendly all silk-based sequential drug delivery system, but also provides an effective tissue engineering functional scaffold for *in-situ* cartilage regeneration.

1. Introduction

Articular cartilage defects have garnered widespread attention due to their high disability [1]. The articular cartilage, being a unique connective tissue devoid of blood vessels, nerves, and lymphatic vessels, has a limited capacity for self-repair following injury [2–5]. Stem cell-based therapeutic strategies are commonly employed in treating cartilage defects; however, several issues still need to be solved, including limited stem cell sources, low viability, complex techniques, high medical costs, and ethical and safety concerns related to clinical translation [6]. Consequently, cell homing therapy, which recruits endogenous stem cells to the injury site, is an alternative strategy [7,8]. Microfracture, a bone marrow stimulation technique, is currently recognized as a

frontline treatment method that is widely utilized to harvest endogenous bone marrow mesenchymal stem cells (BMSCs), providing an ideal autologous cell source for articular cartilage repair [9–11]. Nevertheless, due to the inadequate capacity of microfracture to recruit a sufficient number of stem cells [12,13], the clinical outcomes are unsatisfactory with scar formation and fibrocartilage filling observed at the cartilage defect site [14,15]. Therefore, it is imperative to develop an ideal bioactive scaffold to recruit, program, and guide host cells for *in-situ* tissue regeneration.

In recent years, combining endogenous BMSCs with biomaterials for *in-situ* repair of articular cartilage has emerged as a promising approach [16,17]. The crux of this cell-free cartilage repair lies in constructing an ideal biofunctional scaffold incorporated with growth factors. For

Peer review under the responsibility of KeAi Communications Co., Ltd.

* Corresponding author. Department of Macromolecular Science, Shanghai Stomatological Hospital & School of Stomatology, Fudan University, Shanghai, 200433, China.

** Corresponding author. Department of Orthodontics, Shanghai Stomatological Hospital & School of Stomatology, Fudan University, Shanghai, 200433, China.

E-mail addresses: joyce.zhao.ortho@fudan.edu.cn (B. Zhao), chenx@fudan.edu.cn (X. Chen).

<https://doi.org/10.1016/j.bioactmat.2025.03.005>

Received 13 December 2024; Received in revised form 13 February 2025; Accepted 5 March 2025

2452-199X/© 2025 The Authors. Publishing services by Elsevier B.V. on behalf of KeAi Communications Co. Ltd. This is an open access article under the CC BY-NC-ND license (<http://creativecommons.org/licenses/by-nc-nd/4.0/>).

instance, Xuan et al. developed a poly(glycerol sebacate)-based shape-memory scaffold integrated with the bioactive factor kartogenin (KGN), which successfully promoted chondrocyte proliferation and cartilage regeneration [18]. This scaffold not only exhibited excellent biocompatibility and mechanical properties but also enabled minimally invasive implantation via its shape-memory functionality, offering a novel strategy for cartilage repair. Silk fibroin (SF) is a biomaterial derived from *Bombyx mori* silkworms and approved by the U.S. Food and Drug Administration for clinical use [19], which drawn extensive attention in tissue engineering due to its excellent biocompatibility, non-immunogenicity, and controllable degradability [20–22]. Additionally, as a unique amphiphilic block copolymer, SF is regarded as an effective carrier for both hydrophilic and hydrophobic drugs [23,24], promising significant potential in the field of drug loading and release.

In addition to biomaterials, active factors capable of recruiting endogenous BMSCs and promoting their chondrogenic differentiation are pivotal for cartilage repair. Recent studies have demonstrated that certain peptides can regulate the migration and homing of mesenchymal stem cells. Among them, PFSSTKT (PFS) is a short peptide comprising seven amino acids identified through phage display technology [12, 25–27], and it has successfully bind to various biological scaffolds to form a BMSCs-specific homing scaffold system, achieving satisfactory results both *in vitro* and *in vivo* without species-specificity [28,29]. It has been indicated that PFS-modified gelatin methacrylate (GelMA) hydrogels can accelerate cartilage defect repair primarily owing to the recruitment of BMSCs via PFS [27]. Luo et al. proposed an encapsulation-free triboelectric scaffold that enhances cartilage regeneration through dynamic hydrophilicity and electrical stimulation [30]. By leveraging its porous architecture and electrical cues, this scaffold effectively facilitated BMSC migration and chondrogenesis, providing a promising approach for combining electrical stimulation with biomaterial-based cartilage repair.

Furthermore, maintaining a chondrogenic microenvironment for migrating BMSCs is crucial. KGN, a small heterocyclic compound, has shown strong potential in promoting stem cell differentiation into chondrocytes, playing a key role in cartilage regeneration [29,31]. Compared to protein factors commonly used in osteochondral defect repair, such as transforming growth factor- β (TGF- β) and bone morphogenetic protein (BMP), KGN is more affordable, stable, and controllable, holding greater application potential in clinical [32]. Moreover, it has been indicated that KGN facilitates articular cartilage repair and regeneration by upregulating the expression of aggrecan (ACAN) and collagen type II (COL II) in hyaline cartilage through activation of the core-binding factor- β (CBF- β)/runt-related transcription factor-1 (Runx1) signaling pathway [33,34], thereby avoiding the immunogenicity, instability, and short half-life associated with bioactive factors. Liu et al. demonstrated the potential of motion-induced piezoelectric stimulation for cartilage regeneration, highlighting the application of mechanical stimuli in cartilage repair [35]. By combining piezoelectric scaffolds with exercise therapy, they achieved significant repair of knee cartilage defects in rabbits, underscoring the clinical translation potential of this integrated methodology.

The ideal scenario in cartilage repair involves the early release of drugs that recruit BMSCs, followed by sustained release of chondrogenic bioactive factors to induce the recruited BMSCs to differentiate into chondrocytes [36–38]. Chen et al. have developed a SF coating on gelatin sponge by spin coating, which is loaded with matrix derived factor-1 (SDF-1) and TGF- β 1 to achieve sustained release of multiple factors. However, there is a problem that these two factors cannot be released sequentially [36]. Zhang et al. have loaded E7 peptide and KGN into SF/PVA nanospheres at different concentrations and then incorporated these nanospheres into a SF scaffold to achieve sequential drug release [37]. Such a preparation method is rather complicated and requires multiple matrices for sequential drug release. Mao et al. separately introduced TGF- β 1 and E7 into a SF scaffold and coating layer, enabling their sequential release, but this modified approach also faces

challenges such as the use of crosslinking agents and issues related to the immunogenicity, instability, and short half-life of TGF- β 1 [38]. Notably, treating cartilage defects poses significant risks of pain and inflammation, which can severely impact the repair and regeneration process. Some studies have used dexamethasone (DEX) as a controlled-release drug at inflammatory sites, improving cartilage defect healing [39,40].

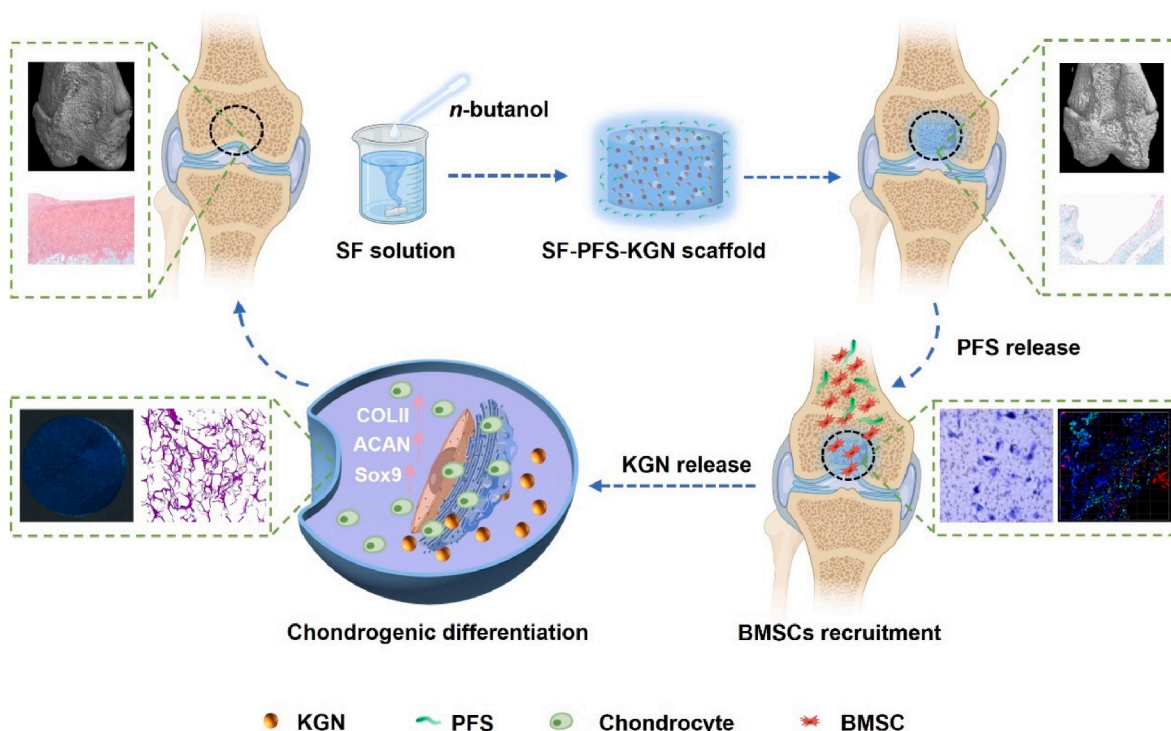
Moreover, ideal tissue engineering constructs should exhibit mechanical properties similar to those of the defective tissue (the tensile strength of cartilage tissue generally ranges between 0.8 and 25 MPa, and its compressive modulus is typically between 0.1 and 2 MPa) [41]. However, many studies have indicated that pristine SF scaffolds exhibit poor mechanical performance, failing to meet the requirements for cartilage defect repair [42,43]. Consequently, there is a necessity to adopt a simple, eco-friendly approach to develop SF scaffolds that not only enhance mechanical properties but also facilitate sequential drug release.

In our recently published work, we integrated several main components of the natural cartilage extracellular matrix (ECM), such as chondroitin sulfate, hyaluronic acid, and collagen type I, into the SF to prepare a tri-layered composite scaffold. The goal was to repair cartilage defects using only substances originally present in the body, and this approach has yielded promising results [19]. However, the entire preparation process of the scaffold is relatively complex, and it requires *in vitro* cultivation of chondrocytes on the SF scaffold before implantation, making the entire experimental process even more complicated. Herein, we adopted another strategy by incorporating drugs with sustainable release capabilities into the SF scaffold, which can be directly implanted into the body without the need for *in vitro* cell culture. An SF scaffold with enough mechanical strength and capable of sequential drug release for *in-situ* cartilage regeneration was developed based on our unique alcohol addition-freezing preparation method [22]. Initially, KGN and DEX were physically adsorbed onto the SF scaffold, enabling the long-term release of KGN and DEX within the scaffold. Subsequently, a SF solution loaded with PFS was coated onto the surface of the SF-KGN scaffold to form a drug-loading layer, facilitating the early and fast release of PFS. The ability of PFS to recruit BMSCs both *in vitro* and *in vivo* was validated and the capacity of KGN to promote the chondrogenic differentiation of BMSCs *in vitro* was confirmed. Finally, the drug-loaded SF scaffold was applied to rat knee joint cartilage defects to investigate its role in enhancing cartilage repair (Scheme 1).

2. Results and discussion

2.1. Preparation and characterization of SF scaffolds

SF scaffolds have been studied for many years as a tissue engineering material, but as materials for cartilage and bone repair, their applications have not made significant breakthroughs due to the poor mechanical properties obtained by traditional preparation methods. The alcohol addition-freezing method invented in our laboratory has effectively improved the mechanical properties of the obtained SF scaffolds, bringing it one step closer to clinical application [22]. As illustrated in Fig. 1a, the SF-PFS-KGN scaffold primarily consists of a SF scaffold with physically adsorbed DEX and KGN, and a SF coating layer containing PFS. The specific preparation conditions for the SF-PFS-KGN scaffold and other scaffolds are detailed in Table S1. In this study, DEX is used as an anti-inflammatory agent, and it is not the focus of subsequent experiments. In our previous work, we have extensively discussed the preparation parameters of the SF scaffold, as well as the effects of pore size, porosity, and mechanical properties on cell growth [19]. Based on these findings, a SF scaffold with a pore size of 100 μ m and a porosity of 95 % was selected for this study. The morphology of the scaffolds with/without the coating was observed by scanning electron microscopy (SEM), which shows that the SF solution was uniformly coated on the scaffold surface. To investigate whether the solution infiltrated the interior and affected the pore structure, the cross-sectional morphology



Scheme 1. Schematic illustration of the design of SF-PFS-KGN scaffold for repairing cartilage defects.

of the scaffolds was investigated. The results indicated that the SF solution was uniformly adsorbed on the pore walls, while the entire SF scaffold retained its three-dimensional porous structure without significantly affecting the pore size (Fig. 1b, Fig. S1a).

Moreover, good porosity and water content are conducive to cell growth. Therefore, the porosity and water content of scaffolds with/without the coating were further analyzed. As shown in Fig. 1c, the porosity of the scaffold decreased from the pristine SF group ($94 \pm 1\%$) to the SF-PFS group ($87 \pm 2\%$), the SF-KGN group ($85 \pm 1\%$), and the SF-PFS-KGN group ($83 \pm 6\%$); the water content decreased from the pristine SF group ($90 \pm 1\%$) to the SF-PFS group ($82 \pm 1\%$), the SF-KGN group ($81 \pm 1\%$), and the SF-PFS-KGN group ($83 \pm 2\%$) (Fig. 1d). Despite the decrease in porosity and water content due to the coating, the overall scaffold still maintained good porosity and hydrophilicity.

Mechanical property tests of scaffolds with/without the coating showed that the compressive modulus increased from the pristine SF group (301 ± 25 kPa) to the SF-PFS group (589 ± 96 kPa), the SF-KGN group (579 ± 51 kPa), and the SF-PFS-KGN group (743 ± 60 kPa) (Fig. 1e and f), the reason for the increase of compressive modulus after coating was attributed to the formation of a dense SF film outside the scaffold, which enhanced the mechanical properties of the whole scaffold. All data were in the range of native cartilage (100–2000 kPa) [41]. It is noteworthy that after coating the weight of the SF scaffold increased by 8 mg (only about 20 % increase), yet showed a nearly 2-fold increase in the compressive modulus. This indicates that the coating not only enables drug loading and release from different regions (coating and scaffold interior) but also significantly enhances the mechanical properties of the scaffold (Fig. S1b). The SF scaffolds with added coatings exhibit a three-dimensional porous structure, high porosity, high water content, and excellent mechanical properties. Therefore, the subsequent experiments utilize the coating strategy, wherein the SF scaffold without PFS uses pure SF solution as the coating.

2.2. Sequential drug release from SF scaffolds and degradation of SF scaffolds

In cartilage repair, scaffold materials need to recruit endogenous BMSCs and subsequently promote their chondrogenic differentiation continuously; thus, the sequence and duration of drug release are critically important [38]. To evaluate the capability of the coating-mediated sequential drug release in SF scaffolds, UV spectrophotometry was applied to quantify the drug release (100 μ g of each drug was used for this release determination due to the detection limit of the UV spectrophotometer) (Figs. S1c–f). As shown in Fig. 2a, PFS release reached 93 % within the first ten days, facilitating the early recruitment of BMSCs. Meanwhile, the release of KGN gradually increases over time, maintaining a sustained and slow release for at least 28 days (with a cumulative release of approximately 71 % at day 28), indicating a sustained release over an extended period consistent with the timeline required for cartilage repair. Concurrently, DEX also demonstrated a release duration of up to 28 days, aiding in the alleviation of inflammation associated with the cartilage repair process. The relatively quickly release of PFS because it was in the coating layer. In the meantime, the coating layer effectively prevented the rapid release of KGN and DEX within the scaffold in the initial stage. As the coating gradually degraded over time, its inhibitory effect on drug release weakened and eventually disappeared, thereby achieving a sustained-release effect that matches the biological process of cartilage repair.

The biodegradation performance of scaffolds is a crucial factor to consider in cartilage repair. *In vitro* enzyme degradation experiments indicated that SF scaffolds with/without coatings exhibited similar degradation behaviors. However, the uncoated scaffolds degraded more rapidly (Fig. 2b). This can be attributed to the dense SF coating layer, which slightly hinders degradation. The ideal degradation time must match the formation of new tissue [19]. Therefore, both the coated and uncoated SF scaffolds (10 mm in diameter, 4 mm in thickness) were stained with Rhodamine B isothiocyanate and implanted subcutaneously in rats. Tissue samples were collected after 4 and 8 weeks of

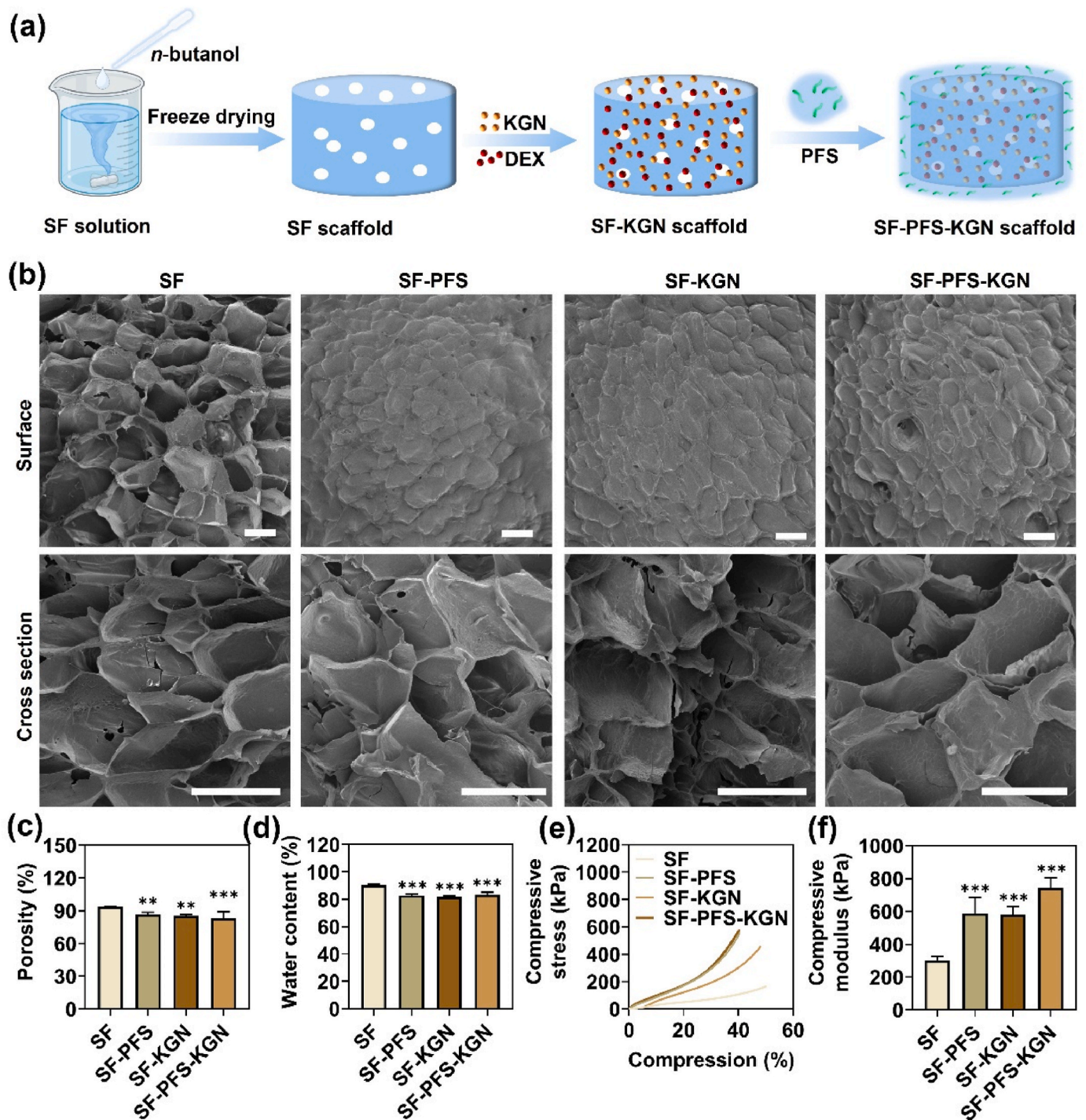


Fig. 1. Preparation and characterization of different SF scaffolds. (a) Preparation of SF-PFS-KGN scaffold. (b) SEM images (scale bar = 100 μm). (c) Porosity. (d) Water content. (e) Compression curves. (f) Compressive modulus. Data are presented as mean ± SD, *n* = 3. Compared with the pristine SF group: ***p* < 0.01, ****p* < 0.001.

implantation, respectively (Fig. S2). As shown in the confocal laser scanning microscopy (CLSM) image, compared to the control group (not implanted subcutaneously), both the fluorescence area of the SF scaffolds with and without the coating layer decreased after 4 weeks. However, the fluorescence area of the coated scaffolds was larger than that of the uncoated scaffolds, indicating that more of the coated scaffolds remained undegraded. After 8 weeks, the fluorescence of all the SF scaffolds was almost undetectable, indicating nearly complete degradation (Fig. 2c). Quantitative analysis of the fluorescence area showed that, at 4 weeks post-implantation, the uncoated SF scaffolds lost about

77 % of their total volume, significantly more than the approximately 54 % degradation observed for the coated scaffolds. By 8 weeks, the degradation of the uncoated scaffolds was about 86 %, while that of the coated scaffolds was about 77 %, with no statistical difference between them (Fig. 2d). The slightly slower early-stage degradation of the coated scaffolds is likely due to the initial degradation of the denser surface coating, followed by the degradation of the scaffold matrix. This process supports the early release of PFS through the degradation of the coating, providing experimental evidence for the intended early release of PFS.

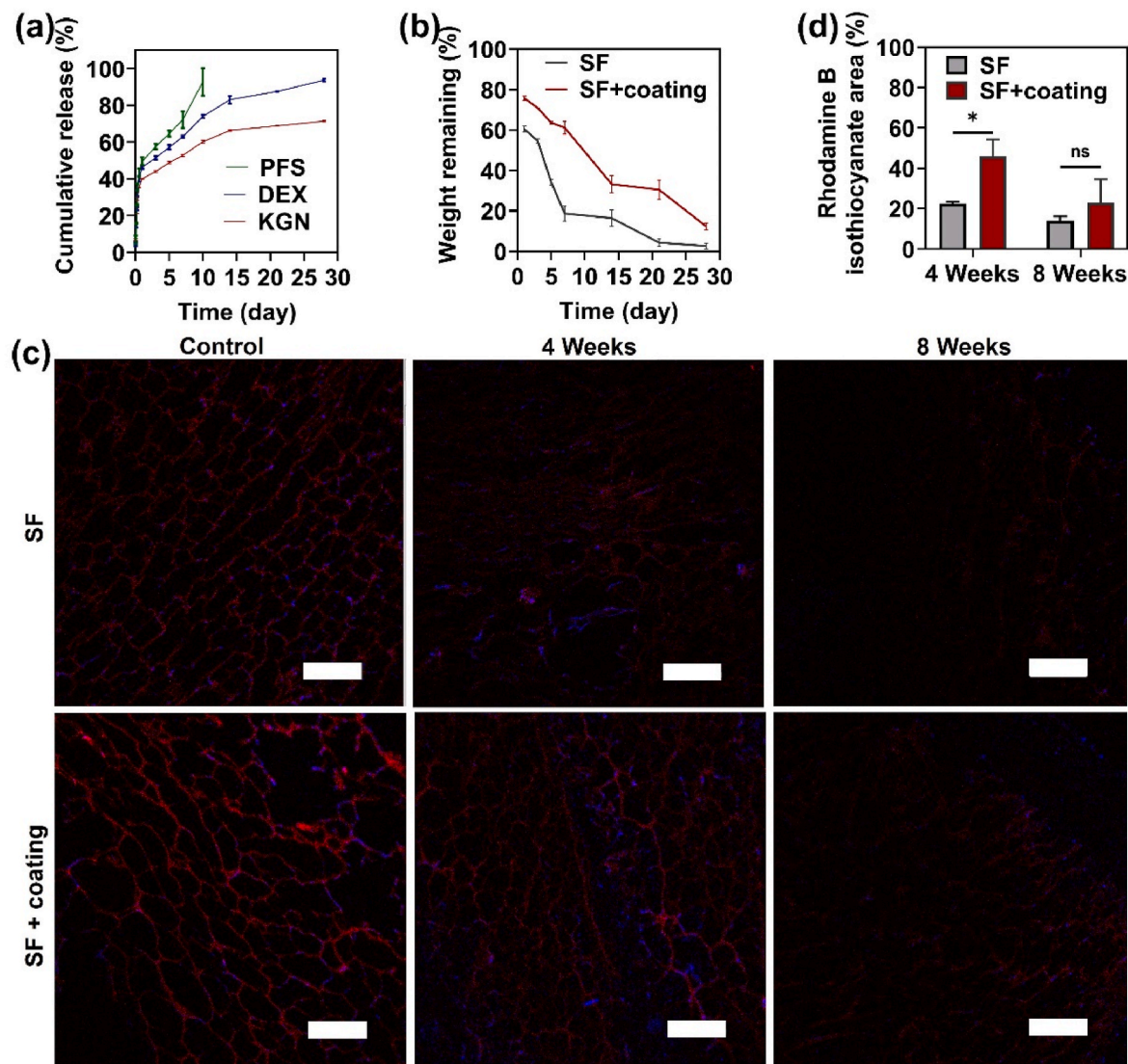


Fig. 2. Drug release, *in vitro* and *in vivo* degradation behavior of SF scaffolds. (a) Cumulative release of PFS, DEX, and KGN in PBS solution at 37 °C. (b) Enzymatic degradation behavior of SF scaffold with/without coating *in vitro*. (c) Confocal laser scanning microscope (CLSM) images of SF scaffold with/without coating degraded *in vivo* for 4 and 8 weeks. (d) Quantitative analysis of rhodamine residual areas of SF scaffold with/without coating (scale bar = 200 μ m). Data are presented as mean \pm SD, $n = 3$. * $p < 0.05$, ns represent no significant different.

2.3. *In vitro* and *in vivo* biocompatibility of SF scaffolds

To decide drug concentrations used *in vitro* and *in vivo* experiments, 2, 10, 50, and 100 μ g/mL of PFS, DEX, and KGN were selected for screening experiments. Briefly, various concentrations of the drugs were co-cultured with cells for 1 and 3 days, followed by live/dead staining and CCK-8 assays to determine the optimal drug concentrations (Fig. S3). The results indicated that after 1 day of cell culture, live cells (green) were observed across all concentration conditions, with almost no dead cells (red), and cell viability was above 90 % (Figs. S3a and b). After 3 days of culture, cells exhibited good viability (>90 %) across all PFS (2–100 μ g/mL) and most KGN concentrations (2–50 μ g/mL). However, increasing DEX concentrations led to a significant increase in the density of dead cells, and cell viability decreased to 68 % at a concentration of 100 μ g/mL (Figs. S3c and d). Thus, PFS (100 μ g/mL), DEX (2 μ g/mL), and KGN (2 μ g/mL) were selected as the drug concentrations for subsequent preparation of the drug-loaded SF scaffold according to the screening results and the published work as well [27,37–39,43,44].

The survival and robust growth of cells on scaffolds are prerequisites for tissue repair and regeneration. To evaluate the biocompatibility of SF

scaffolds, rat bone marrow mesenchymal stem cells (rBMSCs) were co-cultured with the scaffolds for 3 and 7 days, followed by live/dead staining to assess cell growth. The results showed that rBMSCs cultured within each scaffold exhibited high cell viability, with almost no dead cells observed (Fig. 3a). Semi-quantitative analysis of cell viability indicated that cell viability on all scaffold groups was greater than 90 %, with no significant differences, suggesting that all scaffold groups support cell survival and growth (Fig. 3b).

To further confirm cell viability, the proliferation of rBMSCs co-cultured with different SF scaffolds was assessed using the CCK-8 assay on days 1, 3, and 7. The results indicated that rBMSCs proliferated rapidly over time within each scaffold group. There were no significant differences in cell proliferation among the scaffold groups after 1 day of culture; however, on days 3 and 7, the proliferation of cells on the SF-PFS, SF-KGN, and SF-PFS-KGN scaffolds was significantly higher than that on the pristine SF scaffolds (Fig. 3c). These results suggest that PFS and KGN can promote the proliferation of rBMSCs on the scaffolds. On days 3 and 7, the cells were stained with phalloidin (red) for the cytoskeleton and DAPI (blue) for the nucleus, followed by observation of cell adhesion and growth morphology under CLSM. The results showed

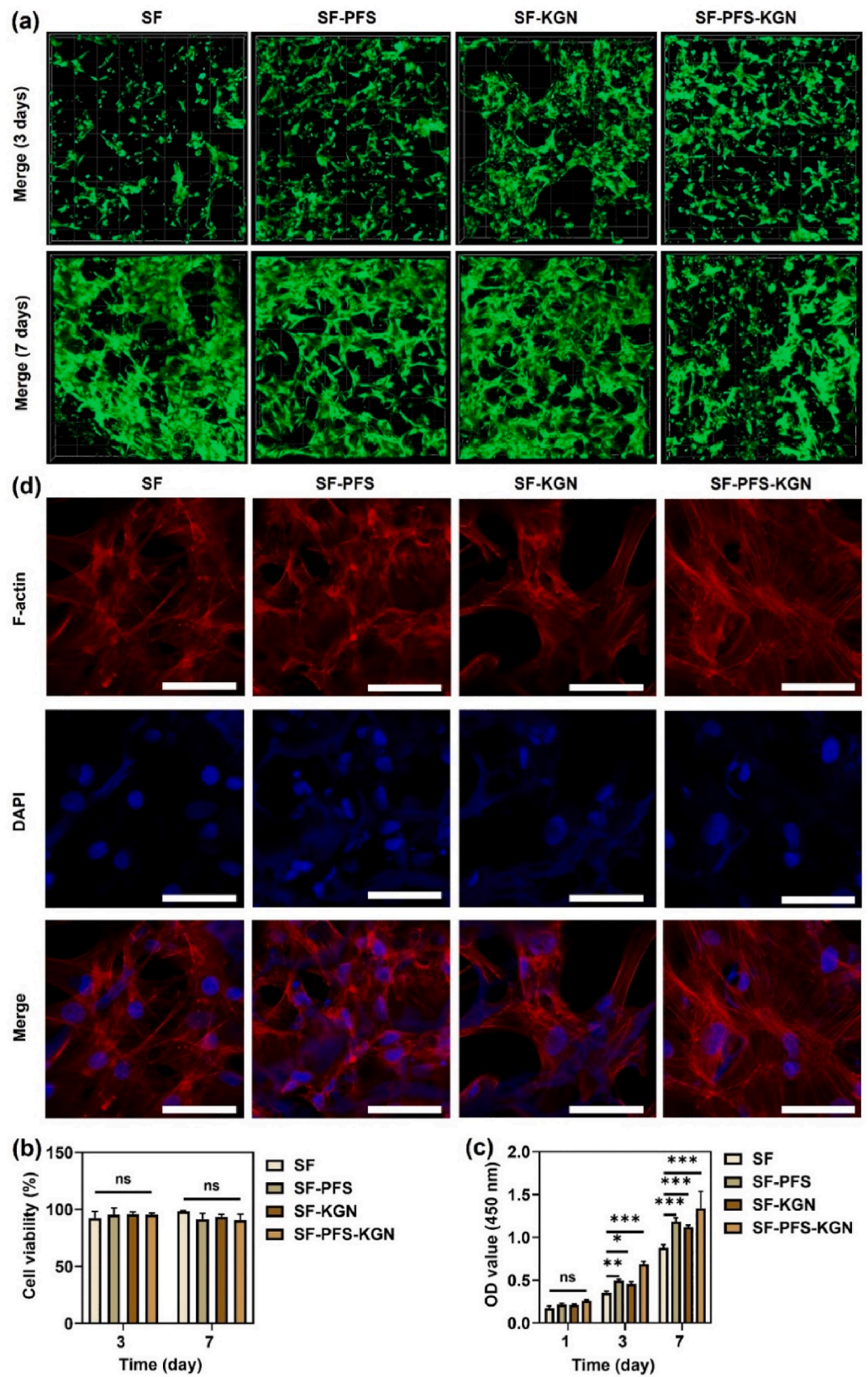


Fig. 3. Biocompatibility of different SF scaffolds. (a) CLSM images of rBMSCs cultured on SF-PFS-KGN scaffolds after 3 and 7 days by live/dead assay. (b) Semi-quantitative analysis of rBMSCs viability on different SF scaffolds by live/dead assay. (c) Cell viability of rBMSCs on different SF scaffolds after 1, 3 and 7 days by CCK-8 assay. (d) CLSM images of microfilament skeleton of rBMSCs cultured on SF-PFS-KGN scaffold after 7 days (red indicates F-actin stained with phalloidin and blue indicates nuclei stained with DAPI (scale bar = 50 μm). Data are presented as mean ± SD, n = 3. *p < 0.05, **p < 0.01, ***p < 0.001, ns represents no significant difference.

that rBMSCs were well dispersed and adhered within all SF scaffolds. As time progressed, the spreading area of rBMSCs within each scaffold group increased, and the cells exhibited spindle and pseudopodial morphologies (Fig. 3d, Fig. S4), indicating that the addition of PFS and KGN do not affect cell adhesion and growth on SF scaffolds.

To better evaluate the biocompatibility and *in vivo* tissue response of SF scaffolds, SF scaffolds with/without coating were implanted into the subcutaneous tissue of rats. The macroscopic appearance of the SF scaffolds after 14 days post-implantation is shown in Fig. S5a. The healthy tissue was observed surrounding both types of scaffolds, with a rich vascular network and no significant inflammatory response. Hematoxylin and eosin (H&E) staining (Fig. S5b) revealed a small number of inflammatory cells around each scaffold, indicating a mild inflammatory response, but no significant tissue necrosis was observed. Additionally, fibroblasts were observed to grow inside the porous scaffolds, and new blood vessel formation was observed at the interface between the tissue and the porous scaffolds (indicated by arrows in Fig. S5b). These results suggest that, regardless of coating, SF scaffolds exhibit good biocompatibility both *in vitro* and *in vivo*, facilitating cell ingrowth from the scaffold surface through the pores into the interior.

2.4. Recruitment of BMSCs by SF scaffolds

Pristine SF scaffold was regarded as a control group to investigate the effect of addition of drugs on the ability of the drug-loaded SF scaffolds to recruit the BMSCs. Transwell assay was adopted to verify the migration of rBMSCs toward different scaffolds *in vitro* (Fig. 4a). The results showed that after adding the extract of four SF scaffold groups to the lower chamber, the number of rBMSCs migrating after 24 h was significantly higher in the SF-PFS group compared to the pristine SF and SF-KGN groups, while the number of migrating cells in the SF-PFS-KGN group was significantly higher than in the SF-PFS group (Fig. 4a and b). These findings indicate that both the SF-PFS and SF-PFS-KGN groups can promote rBMSC migration, with the SF-PFS-KGN group demonstrating a superior effect.

The ability of different SF scaffold groups to recruit rBMSCs was further investigated *in vivo*. CD29 and CD90 were selected as positive markers for the detection of BMSCs according to the literature [12,27,44]. After implantation for 1 week, the number of CD29 and CD90 double-positive cells was significantly higher in the SF-PFS and SF-PFS-KGN groups compared to the other groups (Fig. 4c and d), with the SF-PFS-KGN group showing a significantly higher number than the SF-PFS group. These results are consistent with the *in vitro* findings, further confirming that the SF-PFS-KGN scaffold has the optimal capacity to recruit rBMSCs.

2.5. Chondrogenic differentiation of BMSCs by SF scaffolds

To investigate the chondrogenic differentiation capacity of BMSCs on pristine SF, SF-PFS, SF-KGN, and SF-PFS-KGN scaffolds *in vitro*, BMSCs were cultured with each SF scaffold in chondrogenic medium for 14 days, followed by Alcian Blue staining to assess glycosaminoglycans (GAGs) deposition. As shown in Fig. 5a, the SF-KGN and SF-PFS-KGN groups exhibited stronger staining compared to the pristine SF and SF-PFS groups. The staining intensity was further quantified by measuring the absorbance of the eluted dye at 630 nm. Fig. 5b shows that the GAGs content in the SF-KGN and SF-PFS-KGN groups was significantly higher than that in the pristine SF and SF-PFS groups, with the SF-PFS-KGN group having the highest content, indicating its significant chondrogenic induction capability.

The expression of chondrogenic-related genes COL II, ACAN, and sex-determining region of Y chromosome-box transcription factor 9 (Sox9) in BMSCs cultured with pristine SF, SF-PFS, SF-KGN, and SF-PFS-KGN scaffolds were further assessed by quantitative reverse transcription-polymerase chain reaction (RT-qPCR). As shown in Fig. 5c, after culturing BMSCs with each scaffold group in a chondrogenic medium for

3, 7, and 14 days, the expression of chondrogenic-related genes in the SF-PFS-KGN group was significantly higher than in the other groups. Specifically, compared to the pristine SF scaffold, after 14 days of culture, the levels of COL II, ACAN, and Sox9 genes in rBMSCs of the SF-PFS-KGN group were approximately 75, 50, and 38 times higher, respectively. Additionally, the expression of COL II, ACAN, and Sox9 in the SF-PFS-KGN scaffold showed a significant increase after 7 and 14 days of culture compared to 3 days. Specifically, COL II increased by 1.5-fold and 5.6-fold, ACAN increased by 1.7-fold and 3.6-fold, and Sox9 increased by 1.2-fold and 2.3-fold.

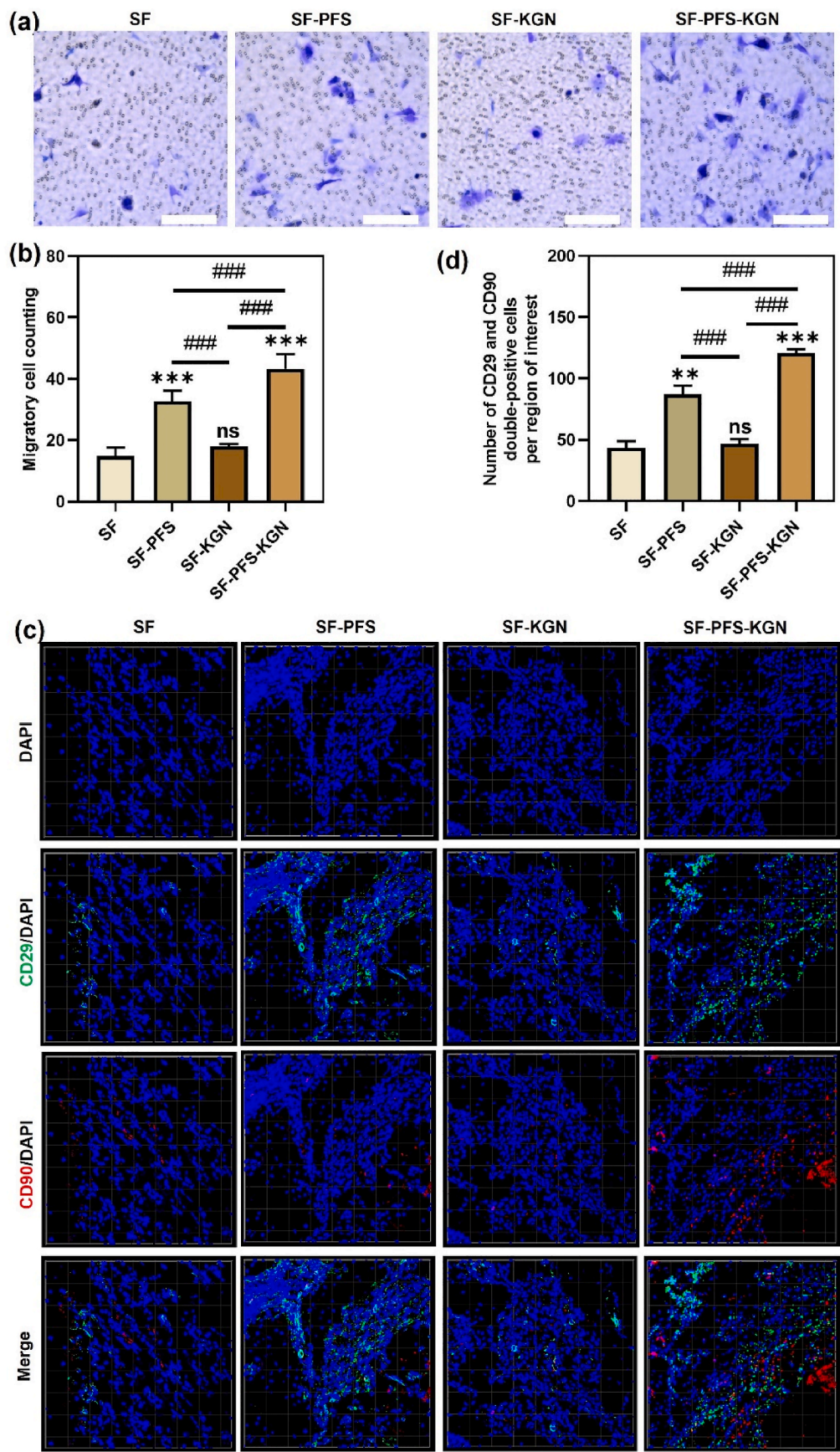
To further analyze the chondrogenic capacity of the SF scaffolds *in vitro*, histological and immunohistochemical analyses were performed after 14 days of co-culture (Fig. 5d). H&E staining results showed that the cell density in the SF-PFS-KGN scaffold group was higher than in the other groups, with more cells and matrix filling the scaffold pores. Additionally, immunohistochemical detection of COL II expression indicated that the SF-PFS-KGN group significantly promoted COL II deposition. According to these results, it can be concluded that the SF-PFS-KGN scaffold provides a favorable microenvironment for the chondrogenic differentiation of rBMSCs.

2.6. Macroscopic evaluation of *in vivo* cartilage repair with SF scaffolds

A cartilage defect model (2 mm in diameter and 2 mm in thickness) was used to evaluate the cartilage regeneration ability of different SF scaffolds (pristine SF, SF-PFS, SF-KGN, and SF-PFS-KGN) compared to a blank group (untreated). The treatment protocol and *in vivo* scaffold implantation for the cartilage defect are shown in Fig. 6a. Macroscopic results (Fig. S6a) showed the defects in the blank group remained evident with almost no new cartilage filling after 4 weeks of operation. The pristine SF, SF-KGN, and SF-PFS groups showed slightly better outcomes, with scaffolds and new tissue visible in the defect sites. However, the surface of the regenerated tissue is uneven and the boundary is unclear, indicating that its repair ability is limited. In contrast, the SF-PFS-KGN group exhibited the best performance, with the defect site largely filled with new tissue and no obvious scaffold presence, indicating that the newly formed cartilage in the scaffold had well integrated with the surrounding host cartilage.

At 8 weeks post-operation, the cartilage defect repair improved in all groups, with varying degrees of new cartilage ingrowth. However, the blank group showed uneven tissue growth with noticeable voids. The pristine SF, SF-KGN, and SF-PFS groups exhibited insufficiently uniform new tissue filling, and their repair outcomes were still inferior to those of the SF-PFS-KGN scaffold group. Additionally, the International Cartilage Repair Society (ICRS) scores were consistent with the macroscopic evaluation results, with the SF-PFS-KGN group scoring significantly higher than the other groups at both 4 and 8 weeks post-operation (Figs. S6b and c). Moreover, the overall cartilage repair assessed by the ICRS score indicated that the cartilage repaired (or grown) in the SF-PFS-KGN group approached normal (grade 2) (Table S3). Therefore, the macroscopic observation of repaired cartilage tissue suggests that the implantation of the SF-PFS-KGN scaffold can effectively promote cartilage defect regeneration.

The three-dimensional views, coronal sections, sagittal sections, and transverse sections of the tissue samples reconstructed by micro-CT are shown in Fig. 6b, c and Fig. S7a. The images reveal that the repair effects of the pristine SF group, SF-PFS group, SF-KGN group, and SF-PFS-KGN group at 4 and 8 weeks post-operation showed significant improvement compared to the control group. However, the pristine SF group, SF-PFS group, and SF-KGN group still exhibited noticeable unrepaired areas (red square sections) at 4 weeks post-operation, and the cartilage layer had voids. Although the therapeutic effect improved by 8 weeks after implantation, a small number of voids in the cartilage layer still remained. In contrast, the SF-PFS-KGN group was almost entirely filled with well-integrated, cartilage-like new tissue, with a smooth and continuous cartilage layer. The quantitative data from the micro-CT



(caption on next page)

Fig. 4. *In vitro* and *in vivo* recruitment of rBMSCs by different SF scaffolds. (a) Crystal violet staining of the migrated rBMSCs in SF-PFS-KGN scaffolds *in vitro* (scale bar = 100 μ m). (b) Quantitative analysis of the crystal violet staining images, (c) CLSM images of endogenous stem cell migration assay *in vivo*. (d) Number of CD29 and CD90 double-positive cells recruited into the cartilage defect. Data are presented as mean \pm SD, $n = 3$. $^{###}p < 0.001$. Compared with the pristine SF group: $^{**}p < 0.01$, $^{***}p < 0.001$, ns represents no significant difference.

analysis, including bone mineral density (BMD), bone volume fraction (BV/TV), trabecular thickness (Tb.Th), and trabecular number (Tb.N), also corroborated these findings (Fig. 6d–g, Figs. S7b–e). The results showed that, regardless of whether it was 4 or 8 weeks post-operation, there were no significant differences in Tb.Th among all SF scaffold groups. However, the primary indicators of cartilage reconstruction such as BMD (0.31 ± 0.03 g/cm³ at 4 weeks; 0.51 ± 0.03 g/cm³ at 8 weeks), BV/TV (23.2 ± 1.9 % at 4 weeks; 38.8 ± 0.9 % at 8 weeks), and Tb.N (1.62 ± 0.33 mm⁻¹ at 4 weeks; 2.34 ± 0.46 mm⁻¹ at 8 weeks) were significantly higher in the SF-PFS-KGN group compared to the other four groups. These results further confirm that the SF-PFS-KGN group exhibits the best cartilage repair efficacy.

2.7. Histological evaluation

Besides the macroscopic evaluation, the repair of the cartilage defect area with SF scaffolds was further analyzed using histological staining. The histological staining images of normal cartilage are shown in Fig. S8. Generally, cartilage defects are gradually filled with repair tissue over time [32], and the results of macroscopic evaluation shown above confirmed this point. The H&E staining results were also found to be similar to these macroscopic evaluation results (Fig. 7a). At 4 weeks post-operation, the defect areas in the blank group were almost unfilled, while the pristine SF, SF-PFS, and SF-KGN groups showed some filling and regenerative tissue, but the cell arrangement and tissue structure were disorganized. Although the repair effect of the SF-PFS-KGN group at 4 weeks was not very obvious, there was still a noticeable improvement compared to the other groups. Additionally, it was noted that the scaffolds had not yet fully degraded, consistent with the *in vivo* degradation results, which aids in the sustained release of osteoinductive factors during the cartilage repair period.

By the 8th week, the repair had improved, with the SF-KGN group displaying uniformly distributed cells on the surface of the regenerated cartilage tissue, exhibiting a round morphology typical of chondrocytes. Although the cells were not arranged in vertical columns and the new cartilage surface was not smooth, this result still supports the role of KGN in inducing chondrogenesis. In contrast, the SF-PFS-KGN group was almost filled with new tissue, and the newly formed cartilage had well integrated with the original tissue, fully demonstrating that the combined use of PFS and KGN effectively promoted the repair of cartilage defects.

To further differentiate the new cartilage from bone tissue, *Safranin O/fast green* staining, which can distinguish between the basophilic cartilage tissue stained red and the eosinophilic bone tissue stained green, was conducted. As shown in Fig. 7b, at 4 weeks post-operation, the blank group, pristine SF group, SF-PFS group, and SF-KGN group almost had no red layer. With the increase in time, by 8 weeks, the SF-KGN group showed increased *Safranin O* staining intensity, indicating the gradual growth of new cartilage during the repair process, confirming that KGN have played a role in promoting cartilage repair. In the SF-PFS-KGN group, although the new tissue was separated from the surrounding normal tissue at 4 weeks, the surface of the new tissue showed significant red staining. After 8 weeks, more new tissue was stained red in the SF-PFS-KGN group, which had completely fused with the surrounding normal tissue. Notably, when PFS and KGN were used together, the regenerated cartilage had a complete structure, uniformly distributed cells, and increased staining and thickness of the repair tissue, indicating that PFS and KGN had a synergistic effect on cartilage repair. Additionally, the ICRS visual scoring results showed that the overall scores of the SF-PFS-KGN group at 4 and 8 weeks post-operation

were significantly higher than those of the other groups (Fig. 7c and d).

In addition to polysaccharides, COL II is also a major component of articular cartilage. The immunohistochemical staining of COL II in repair tissue indicates that the positive staining in the defect area was not very obvious in the blank group, pristine SF group, and SF-PFS group at 4 and 8 weeks (Fig. 7e). However, the COL II content in the SF-KGN group and SF-PFS-KGN group was higher compared to the blank group, pristine SF group, and SF-PFS at 4 weeks, and it was even more significant at 8 weeks. In addition, the newly formed cartilage tissue in the SF-PFS-KGN group showed obvious staining at 4 weeks, which was significantly better than the other four groups. At 8 weeks, the COL II immunohistochemical staining in the SF-PFS-KGN group showed no significant difference from the non-defective cartilage around, confirming that the SF-PFS-KGN group had a more significant effect on cartilage formation. Besides, the newly formed cartilage in the SF-PFS-KGN group was smooth, and the chondrocytes were arranged in clusters, indicating that the combination of PFS and KGN is indeed conducive to the rapid and efficient formation of new cartilage with structures and deposits similar to original cartilage, confirming that the SF-PFS-KGN scaffold has a strong promotional effect on cartilage repair. In addition, the expression of COL II in the SF-PFS-KGN group was higher than that in the other groups at both 4 and 8 weeks after implantation (Fig. 7f and g). These results also confirm that SF-PFS-KGN has good cartilage repair ability.

3. Conclusion

In this article, a functional SF-PFS-KGN scaffold through a simple strategy was successfully developed, which is composed a DEX and KGN-loaded SF scaffold coating with a PFS-loaded SF layer. This method not only improves the mechanical properties of the SF scaffold but also endows it with the function of sequential and sustained drug release.

The *in vitro* experimental results of BMSC growth on the SF-PFS-KGN scaffold show the scaffold maintained good biocompatibility and cell adhesion, indicating the incorporation of PFS and KGN during the preparation did not have a negative impact. Both *in vitro* cell migration experiments and *in vivo* cell recruitment experiments confirmed that PFS released from the coating of the scaffold promoted the recruitment of BMSCs. In the meantime, *in vitro* cell experiments demonstrated that the KGN released from the SF scaffold significantly promoted the chondrogenic differentiation of BMSCs through increased expression of COL II, ACAN, and Sox9 genes. This lays a solid experimental foundation for subsequent cartilage defect repair with SF-PFS-KGN scaffold.

To further validate its *in vivo* role in promoting cartilage repair, the SF-PFS-KGN scaffold was implanted into a rat knee joint cartilage defect model. Micro-CT and histological studies results demonstrated that the SF-PFS-KGN scaffold significantly promoted the regeneration of cartilage defects by promoting stem cell recruitment and chondrogenic differentiation through the sequential release of PFS and KGN.

In conclusion, the facile preparation procedure, controllable shapes, and easy-to-use properties of the SF-PFS-KGN scaffold provide a promising means for developing cartilage substitutes and promoting *in situ* cartilage regeneration, which could provide guidance for the clinical treatment of cartilage defects.

4. Experimental section

4.1. Preparation of SF scaffolds

The degumming process of *Bombyx mori* silk cocoons was conducted

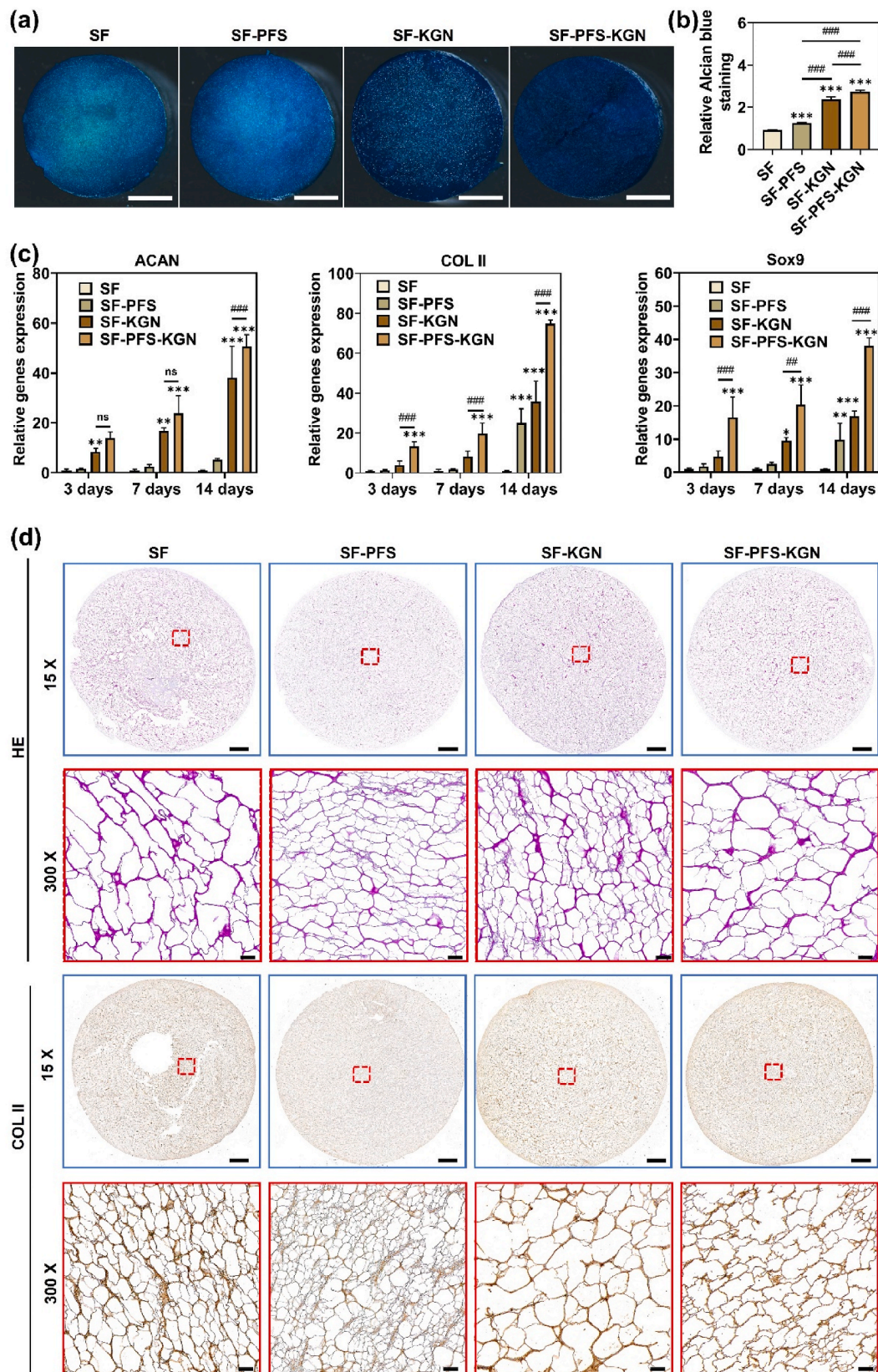


Fig. 5. *In vitro* chondrogenic assays. (a) Alcian blue staining of rBMSC cultured SF-PFS-KGN scaffolds after 14 days of culture in chondrogenic medium (scale bar = 3 mm). (b) Quantification of Alcian blue staining by measuring the absorbance of the eluent at 630 nm. (c) RT-qPCR results of mRNA expression of COL II, ACAN, and Sox9 in rBMSC cultured scaffolds after 3, 7, and 14 days. (d) H&E and COL II staining of rBMSC cultured scaffolds after 14 days (scale bars = 1000 μ m (15x); 50 μ m (300x)). Data are presented as mean \pm SD, n = 3. ###p < 0.01, ###p < 0.001. Compared with the pristine SF group: *p < 0.05, **p < 0.01, ***p < 0.001.

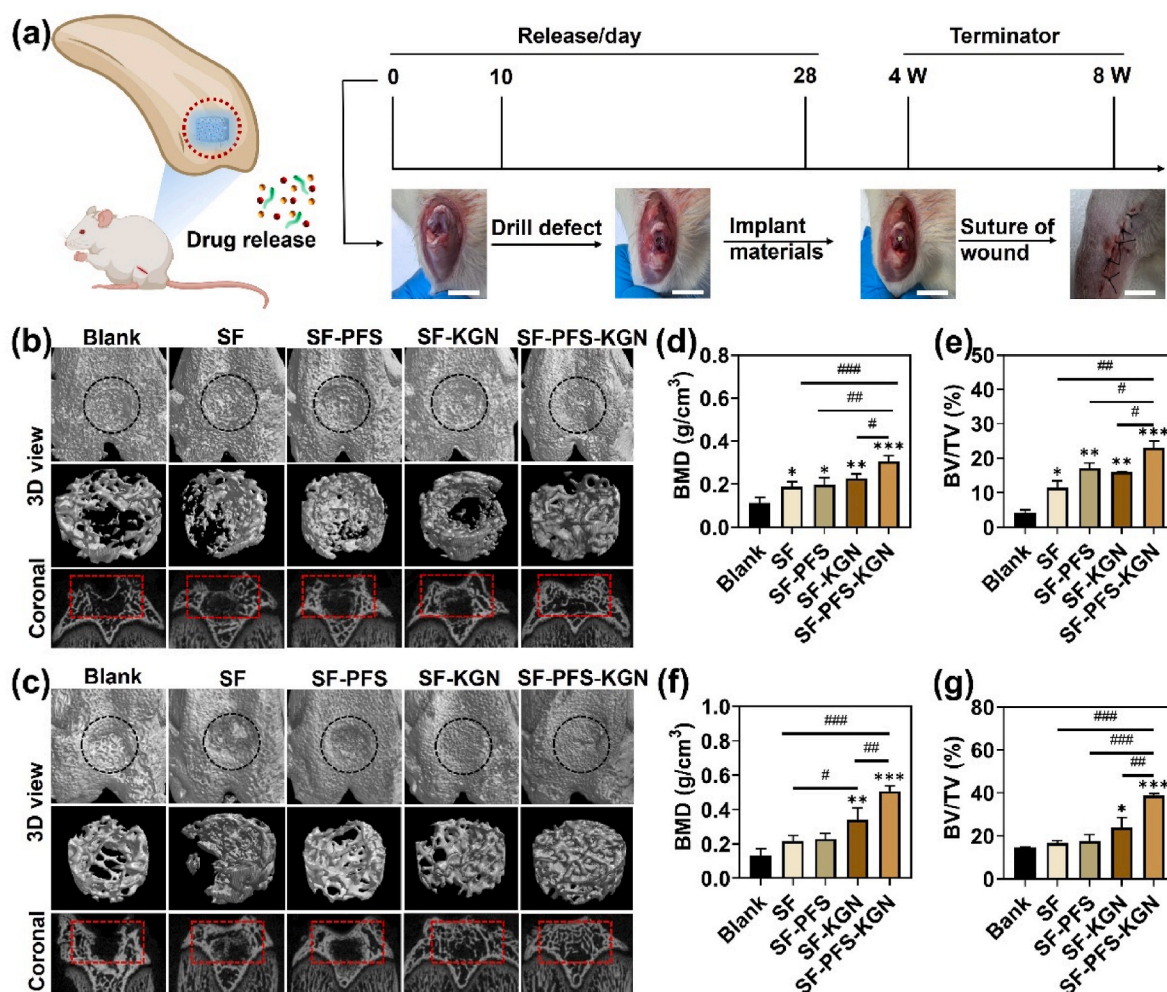


Fig. 6. Evaluation of repaired cartilage defects by different SF scaffolds after 4 and 8 weeks of surgery. (a) Scheme of the scaffolds treatment and implantation process *in vivo*. (b, c) Micro-CT images obtained from 3D reconstruction and coronal view of the repaired joints after 4 and 8 weeks of surgery (black circles and red squares indicate the original defect borders). (d) BMD value after 4 weeks of surgery. (e) BV/TV value after 4 weeks of surgery. (f) BMD value after 8 weeks of surgery. (g) BV/TV value after 8 weeks of surgery. Data are the means \pm SD, $n = 3$. * $p < 0.05$, ** $p < 0.01$, *** $p < 0.001$. Compared with the blank group: * $p < 0.05$, ** $p < 0.01$, *** $p < 0.001$.

according to the previous work [45]. Briefly, the silk was first degummed with a 0.5 wt% Na_2CO_3 aqueous solution at 100 °C for 45 min, followed by thorough rinsing with deionized water. After drying, the extracted silk was dissolved in 9.3 mol/L LiBr aqueous solution at 60 °C for 1 h. The undissolved silk fibers and impurities in the solution were filtered through 8 layers of gauze; then the prepared solution was dialysis against deionized water using a cellulose dialysis membrane (MWCO 12–14 kDa) for 3 days to remove salts. Subsequently, the obtained silk fibroin (SF) solution was centrifuged at 8000 rpm for 10 min. Finally, the SF solution was concentrated with a 12.5 wt% PEG solution to a final concentration of 14 wt% and stored in a 4 °C refrigerator for subsequent use. The solid content of the solution was determined by weighing.

The preparation of the SF scaffold followed the previous method in our group [46,47]. Briefly, *n*-butanol was added dropwise to the SF aqueous solution (*n*-butanol: SF = 1:4 vol ratio) and stirred at room temperature at 400 rpm for 2 min. The obtained solution was poured into a container and frozen at –20 °C for 24 h, then thawed at room temperature and washed with ethanol to completely remove *n*-butanol. Finally, ethanol was displaced with deionized water to obtain the SF scaffold. Unless otherwise specified, the final concentration of SF used in the preparation procedure was 7 wt%.

4.2. Preparation of drug-loaded SF scaffolds

20 μL of KGN and DEX ethanol solutions (100 $\mu\text{g}/\text{mL}$) were carefully dripped onto the SF scaffold to fully adsorb onto the pore walls of the scaffold to make the amount of KGN and DEX was 2 μg , respectively. The scaffold was then freeze-dried for 24 h to obtain the SF-KGN pre-scaffold. The SF-KGN pre-scaffold was immersed in a 20 wt% SF solution containing PFS (2.5 mg/mL) for 10 s, then was fumigated with ethanol for 24 h and freeze-dried to obtain the SF-PFS-KGN scaffold with a PFS coating, in which the PFS amount was approximately 100 μg . The SF-KGN pre-scaffold was coated with SF solution without PFS to obtain the SF-KGN scaffold. Pristine SF and SF-PFS scaffolds were obtained using a similar method. For pristine SF scaffold, only the SF solution was coated on the SF scaffold without any drugs in them. For SF-PFS scaffold, only DEX (100 $\mu\text{g}/\text{mL}$) ethanol solution was dripped onto the SF scaffold and the following procedure was the same as SF-PFS-KGN scaffold. All scaffolds used for cell and animal experiments were sterilized by γ -irradiation (Nuctech, China).

4.3. Characterization of drug-loaded SF scaffolds

4.3.1. Morphological observation

The SF scaffolds from each group were freeze-dried and fractured in

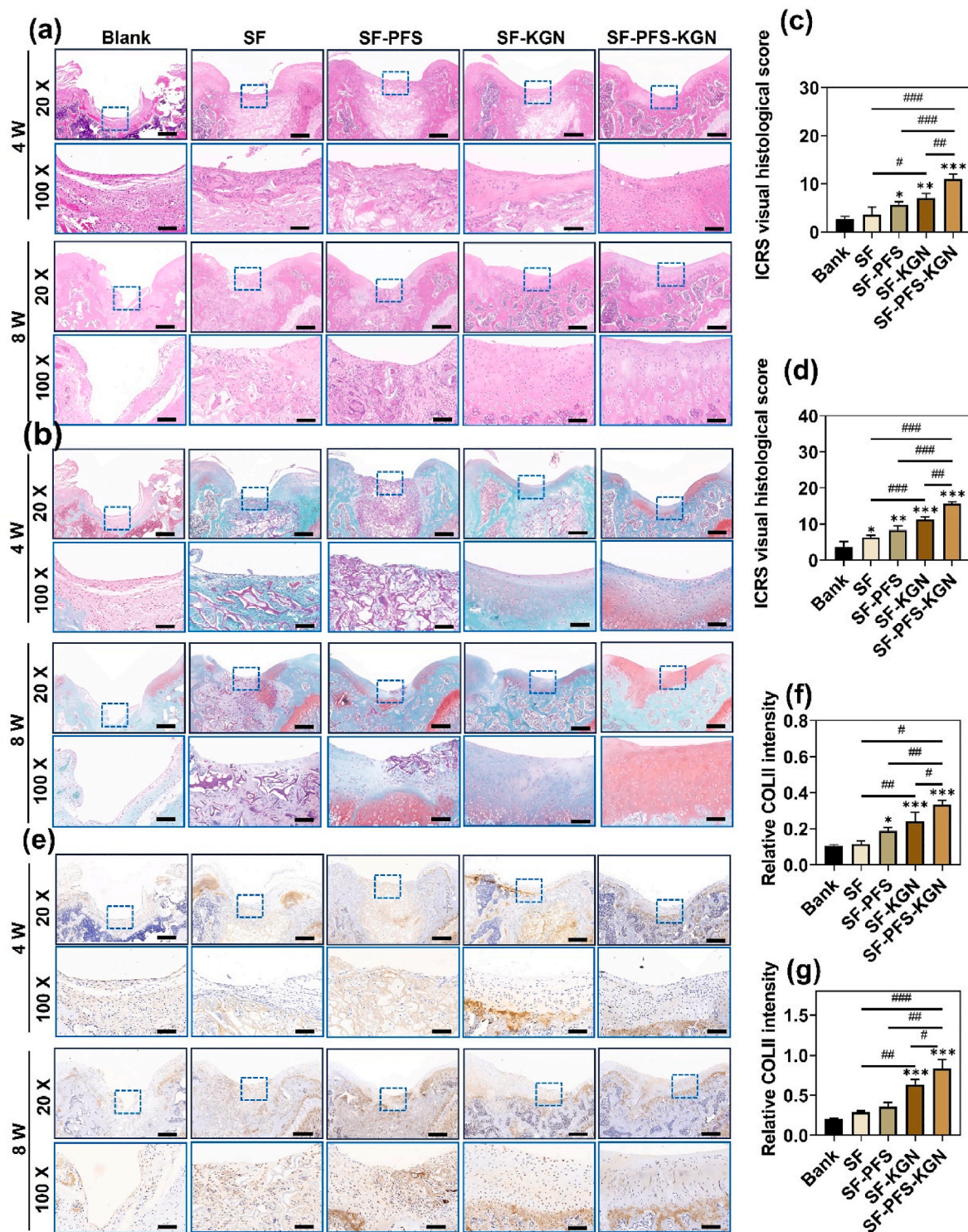


Fig. 7. Histological staining images of cartilage defects after 4 and 8 weeks of operation. (a) H&E staining. (b) Safranin O/fast green staining. (c) ICRS visual histological scoring at 4 weeks. (d) ICRS visual histological scoring at 8 weeks. (e) Immunohistochemical staining (scale bars = 500 μ m (20x); 100 μ m (100x)). (f) Quantitative analysis of the COLII content at 4 weeks. (g) Quantitative analysis of the COLII content at 8 weeks. Data are the means \pm SD, $n = 3$. # $p < 0.05$, ## $p < 0.01$, ### $p < 0.001$. Compared with the blank group: * $p < 0.05$, ** $p < 0.01$, *** $p < 0.001$.

liquid nitrogen, followed by gold sputter coating. The surface and cross-sectional morphology of the scaffolds were observed under an Ultra55 SEM (Zeiss, Germany) at an accelerating voltage of 3 kV. Image J software was utilized to analyze the pore size of the scaffolds. At least 50 randomly selected pores were statistically analyzed, and the results were expressed as mean \pm standard deviation (SD).

4.3.2. Porosity determination

The porosity of the SF scaffold was measured using the liquid displacement method [46]. Hexane was chosen as the displacement solvent since it does not swell or shrink the SF matrix. The SF scaffold after freeze-drying was placed in a volume of hexane solvent, denoted as V1. Under a certain negative pressure, the hexane was allowed to fully

penetrate the scaffold's pores. The volume of hexane at this point was recorded as V2. The scaffold filled with hexane was then removed, and the volume of the solvent was measured as V3. Therefore, the pore volume of the scaffold can be calculated as (V1-V3), and the macroscopic volume of the scaffold as (V2-V3). Thus, the porosity of the SF scaffold can be determined using equation (1):

$$\text{porosity} = \frac{V1-V3}{V2-V3} \times 100\% \quad (1)$$

At least 5 scaffolds were tested for each group, and the results were expressed as mean \pm SD.

4.3.3. Water content

Record the initial dry weight (Wd) of each group of freeze-dried SF scaffolds. Then immerse the samples in deionized water at 37 °C for 24 h, remove the excess water from the surface carefully using filter paper, and reweigh the scaffolds (Ws). The water content of the scaffolds is calculated using equation (2):

$$\text{water content (\%)} = \left[\frac{Ws-Wd}{Ws} \right] \times 100\% \quad (2)$$

A minimum of 5 scaffolds were tested for each group, and the results were expressed as mean \pm SD.

4.3.4. Mechanical test

The mechanical performance of the SF scaffold was measured using an Instron 3365 universal testing machine (Instron, USA). The testing followed the ASTM standard D1621-04a (Standard Test Method for Compressive Properties of Rigid Cellular Plastics) [46]. Before testing, the scaffold was cut into cylindrical shapes with a diameter of 10 mm and a thickness of 4 mm. Compression testing was performed at a loading rate of 5 mm/min under a preload of 0.05 N until a displacement of 50 % strain was reached. Stress-strain curves and compressive modulus were determined using previously reported methods [46]. A minimum of 5 scaffold samples were tested for each group, and the results were expressed as mean \pm SD.

4.3.5. In vitro degradation

First, the initial dry weight (W₀) of each scaffold group was measured. The scaffolds were then placed in 7 mL centrifuge tubes and immersed in a PBS solution containing proteinase XIV (1 U/mL, pH 7.4). The centrifuge tubes were shaken in a temperature-controlled shaker (37 °C, 100 rpm). The solution was changed with a fresh solution every 2 days. At specified time points (1, 3, 7, 14, and 28 days), the scaffolds were removed, rinsed with deionized water, dried, and weighed (W₁). The degradation rate of the scaffold was calculated as the percentage of mass loss using equation (3):

$$\text{Mass loss (\%)} = \left[\frac{W_0-W_1}{W_0} \right] \times 100\% \quad (3)$$

A minimum of 5 scaffold samples were tested for each group, and the results were expressed as mean \pm SD.

4.3.6. Drug release

The SF scaffolds from each group were placed in centrifuge tubes containing PBS buffer. The centrifuge tubes were then placed on a temperature-controlled shaker (37 °C, 100 rpm) for incubation. At specified time points, 1 mL of the PBS buffer was taken out (while simultaneously adding 1 mL of fresh PBS buffer for further incubation) and its absorbance was measured using a Lambda 750 UV-vis spectrophotometer (PerkinElmer, USA). The cumulative drug release was calculated using a standard curve of the drug.

4.4. In vitro biocompatibility evaluation of SF scaffolds

4.4.1. Cell extraction and culture

Primary rat rBMSCs were extracted following the previous methods of our research group [48]. In brief, rBMSCs were extracted from the bone marrow of 4-week-old male *Sprague-Dawley* (SD) rats. The SD rats were euthanized by an overdose of pentobarbital intraperitoneal injection (150 mg/kg) and then soaked in 75 % ethanol for 10 min. The femurs were isolated and the bone marrow cavity was flushed with complete culture medium (α -MEM medium (VivaCell) + 10 % fetal bovine serum (FBS, Gibco) + 1 % penicillin-streptomycin (PS, Gibco)). The collected washings were filtered and centrifuged at 1000 g for 5 min. The cell pellets were resuspended and cultured in a 55 cm² culture dish and placed in a carbon dioxide incubator (5 % CO₂, 37 °C). The culture medium was replaced 2 days later to remove non-adherent cells, and then changed every 3 days. When the cell confluence reached 80–90 % density, it was passed or frozen. The third passage (P3) rBMSCs were used in subsequent experiments.

4.4.2. Live/dead staining

A live/dead cell staining assay using the live/dead cell viability assay kit (Beyotime, Shanghai, China) was performed to assess the viability of BMSCs on different SF scaffolds. In brief, the sterilized SF scaffolds were placed in a 24-well plate. Digestion and centrifugation were performed on BMSCs, and the cells were seeded onto the scaffolds at a density of 5×10^4 cells per scaffold. The plate was then placed in a carbon dioxide incubator (5 % CO₂, 37 °C) for 2 h to allow cell adhesion to the scaffolds. Subsequently, 1 mL of complete culture medium was added to each well and the cells were further cultured for 3 and 7 days, with the culture medium changed every 3 days. At the specified culture time points, the culture medium was removed, and the scaffold-cell complexes were rinsed with PBS. Then, a staining solution containing 1 mM calcein AM and 2 mM ethidium homodimer-1 in 500 μ L was added to each well, and the cells were incubated in a dark room at 37 °C for 30 min. Finally, after rinsing with PBS, images were obtained using a LSM 980 CLSM (Zeiss, Germany). Unless otherwise specified, the size of the SF scaffolds involved in subsequent experiments were all 10 mm in diameter and 2 mm in thickness.

4.4.3. CCK-8 assay

The proliferation of rBMSCs on different SF scaffolds was quantitatively assessed using the CCK-8 assay kit (Beyotime, Shanghai). In the CCK-8 assay, rBMSCs were seeded onto the SF scaffolds at a density of 5×10^3 cells per scaffold. After co-culturing for 1, 3, and 7 days, the culture medium was replaced with 110 μ L of working solution (CCK-8 reagent/culture medium, volume ratio = 1:10) and incubated at 37 °C for 2 h. Then, 100 μ L of the incubation solution was transferred to a new 96-well plate, and the optical density (OD) of the CCK-8 solution at 450 nm was measured using a Cytation 3 multi-mode microplate reader (BioTek, USA).

4.4.4. Cell morphology and adhesion ability

The morphology and adhesion ability of rBMSCs in different SF scaffolds were evaluated using 4',6-diamidino-2-phenylindole (DAPI) (Beyotime, Shanghai) and phalloidin (Cytoskeleton, USA) staining. Specifically, after culturing for the specified time (3 and 7 days), the SF scaffolds were removed. They were washed three times with PBS for 5 min each and fixed with 4 % paraformaldehyde (PFA) at room temperature for 15 min. After discarding the fixative, the scaffolds were washed three times with PBS and incubated with Triton X-100 at room temperature for 10 min. The solution was then discarded, and the scaffolds were washed three times with PBS. The phalloidin staining working solution was prepared according to the instructions, and the scaffolds were incubated in the dark at room temperature for 20 min. Then the staining was terminated by washing with PBS. DAPI staining solution was added to stain the cell nuclei, and the scaffolds were

incubated in the dark for 20 min. After washing three times with PBS, images were obtained using a LSM 980 CLSM (Zeiss, Germany).

4.5. *In vitro* chondrogenic differentiation

4.5.1. *In vitro* cell migration

The ability of the SF scaffolds in each group to recruit BMSCs was determined using a Transwell system (Corning, USA). In the upper and lower chambers of the Transwell culture plate, an appropriate amount of α -MEM medium was added and incubated at 37 °C for 24 h. After removing the medium, the SF scaffolds were placed in the lower chamber, with 3 replicates per group. In the upper chamber, a complete culture medium containing 5×10^4 BMSCs was added (200 μ L per well). After 24 h, the upper chamber was carefully removed, washed three times with PBS, fixed with 4 % PFA for 30 min, and then washed three times with PBS. The cells were stained with 0.1 % crystal violet solution for 30 min, and non-migrated cells were removed by gently wiping them with a cotton swab. The Transwell inserts were rinsed three times with distilled water, dried, and observed and photographed under a microscope. Three random fields were selected for each chamber. The migration quantity of rBMSCs was calculated using Image J software.

4.5.2. Alcian blue staining

rBMSCs were seeded at a density of 1×10^5 cells/scaffold on the SF scaffolds. After incubating in a carbon dioxide incubator for 2 h to allow cell adhesion to the scaffold, complete culture medium was added to continue culture for 2 days before switching to chondrogenic induction medium (α -MEM medium + 10 % FBS + 100 nM dexamethasone + 50 μ g/mL L-ascorbic acid + 1 % ITS supplement + 40 μ g/mL L-proline + 1 mM sodium pyruvate + 10 ng/mL TGF- β 3) further cultured for 14 days, with the medium changed every 3 days. At the specified time points, the scaffolds were removed, washed three times with PBS, and then stained with 1 % Alcian blue solution (pH 2.5). The stained scaffolds were photographed using a stereomicroscope. For quantitative analysis, the stained scaffolds were dissolved in 6 mol/L guanidine hydrochloride (Aladdin, Shanghai) solution, and the absorbance at 630 nm was measured using a multi-mode microplate reader.

4.5.3. RT-qPCR test

BMSCs were seeded on SF scaffolds at a density of 1×10^5 cells per scaffold. After incubating in a carbon dioxide incubator for 2 h to allow cell adhesion to the scaffold, culture medium was added and the cells were cultured for an additional 2 days before switching to chondrogenic induction medium. After chondrogenic culture for 3, 7, and 14 days, the expression levels of COL II, ACAN, and Sox9 were detected using RT-qPCR. In brief, total RNA was extracted from rBMSCs using Trizol reagent (Beyotime, Shanghai). The RNA concentration was quantified using a NanoDrop 2000 UV–vis spectrophotometer (Thermo, USA). One microgram of RNA was reverse-transcribed into complementary DNA (cDNA) using the FastKing RT Kit (Tiangen, China). For RT-qPCR, a 10 μ L reaction solution (5 μ L 2 \times SuperReal PreMix Plus (SYBR Green, Tiangen, China), 0.3 μ L each of forward and reverse primers, 1 μ L cDNA, and 3.4 μ L nuclease-free water) was added to a PCR plate, centrifuged for 1 min to mix, and then amplified and detected using a LightCycler 96 thermal cycler (Roche, Switzerland). Glyceraldehyde-3-phosphate dehydrogenase (GAPDH) was used as the internal reference gene, and the relative expression levels of the target genes were calculated using the $2^{-\Delta\Delta CT}$ method. The primer sequences are provided in Table S2.

4.5.4. Histological staining

BMSCs were seeded on SF scaffolds at a density of 1×10^5 cells per scaffold. After co-culturing for 14 days, the scaffolds were fixed with 4 % PFA, dehydrated, embedded in paraffin, and sectioned into 4 μ m thick slices. After dewaxing and hydration, the slices were stained with hematoxylin and eosin (H&E) for histological examination following standard protocols. Immunohistochemistry was then performed to

evaluate the expression of COL II in the scaffolds. After the paraffin sections dewaxing to water, endogenous peroxidase was removed by treatment with hydrogen peroxide, followed by washing with PBS and sealing the slices. The slices were incubated with the primary antibody against COL II (Servicebio) overnight at 4 °C in a wet box. After washing with PBS, the corresponding secondary antibody was added, and the slices were stained with DAB color developing solution, then images were captured using a Nikon E100 bright-field microscope (Nikon, Japan).

4.6. *In vivo* animal experiment

4.6.1. Surgical procedure

All animal experiments were conducted following the ethical guidelines approved by the Ethics Committee of the Laboratory Animal Science Department of Fudan University (Approval No.202310039S). After intraperitoneal injection of pentobarbital (35 mg/kg), the male SD rats were anesthetized and prepared for surgery. The skin of the right leg was incised to expose the rat knee joint, the joint capsule was cut to dislocate the patella, thereby exposing the articular cartilage. Standard cartilage defects were created using a trephine (2 mm in diameter and 2 mm in depth). After modeling, the prepared SF scaffolds were implanted into the defect areas. Once the scaffolds were confirmed to be firmly implanted, the joint capsule and skin were sutured layer by layer (the right knee joint per SD rat was selected for model establishment). The rats were sacrificed at different time points to collect knee joint samples for the study of *in vivo* BMSCs recruitment and cartilage defect repair. In total, 12 male SD rats (8 weeks old, 200–250 g) were randomly divided into four groups: pristine SF group, SF-PFS group, SF-KGN group, and SF-PFS-KGN group, with 3 rats in each group ($n = 3$). After 1 week surgery, the rats were euthanized by intraperitoneal injection of an overdose of pentobarbital (150 mg/kg), and knee joint specimens were collected for the study of *in vivo* BMSC recruitment. In addition, 50 male SD rats (8 weeks old, 200–250 g) were randomly divided into five groups: the blank group, pristine SF group, SF-PFS group, SF-KGN group, and SF-PFS-KGN group, with 5 rats in each group and two different treatment times (4 weeks and 8 weeks) ($n = 5$). After 4 and 8 weeks of operation, the rats were euthanized by intraperitoneal injection of an overdose of pentobarbital (150 mg/kg), and the distal femoral condyles of the right knee joints were collected for cartilage defect repair.

4.6.2. Endogenous BMSCs recruitment

CD29 and CD90 were used as specific markers for BMSCs, and the recruitment ability of BMSCs to SF scaffolds was detected using immunofluorescence staining [12]. In general, knee joint samples collected in the above process were fixed with 4 % PFA for 30 min and then subjected to paraffin sectioning. The sections were deparaffinized using environmentally friendly dewaxing solution, gradient ethanol, and distilled water, followed by antigen repair using EDTA antigen repair solution. The sections were then blocked with BSA for 30 min. The mixture of primary antibodies CD29 (Servicebio, 1:300) and CD90 (Servicebio, 1:300) was added to the sections and incubated overnight at 4 °C in a wet box. After washing with PBS, the samples were incubated at room temperature in the dark with secondary antibodies conjugated with Alexa Fluor 488 and Fluor 594 (Servicebio, 1:500) for 50 min. Following PBS washing, DAPI (Servicebio) solution was added and incubated at room temperature in the dark for 10 min. After washing with PBS, autofluorescent quencher B solution (Servicebio) was added for 5 min, and rinse with running water for 10 min. The sections were finally sealed with an anti-fade mounting medium. CD29 and CD90 positive cells in the regenerative area were observed using a LSM 980 CLSM (Zeiss, Germany).

4.6.3. Macroscopic evaluation and ICRS scoring

After 4 and 8 weeks of operation, macroscopic observations and photography of the repaired rat knee joints were performed using a

stereomicroscope. The observations included checking for adhesions within the joint, assessing the repair of the articular surface, and noting any changes in the intra-articular tissues. The condition of the implanted scaffold at the defect site was examined, including the size range, color, and smoothness of the repaired cartilage. The integration of the newly formed tissue with the surrounding tissue was observed, and the morphology was evaluated using the criteria set by the International Cartilage Repair Society (ICRS) as described in Table S3. The scoring was independently conducted by three individuals who were not involved in the experiment.

4.6.4. Micro-CT scanning and analysis

The collected knee joint cartilage samples were fixed with 4 % PFA for 24 h and then temporarily stored in 70 % ethanol. A SkyScan 1176 micro-CT (Bruker, USA) was used to scan the cartilage samples to evaluate the regenerated tissue. The scanning parameters were set as follows: voltage 70 kV, current 142 μ A, and resolution 18 μ m. The collected scan data were reconstructed and analyzed using CTan software. The BMD, BV/TV, Tb.Th, and Tb.N in the cartilage defect area were calculated to evaluate the cartilage reconstruction.

4.6.5. Histological evaluation

Following micro-CT scanning, the samples were subjected to decalcification using a 10 % ethylenediaminetetraacetic acid (EDTA, pH 7.4, Servicebio) solution. The EDTA solution was refreshed every two days, and the process was continued for four weeks. Subsequently, the samples underwent dehydration treatment. The tissue samples, which included the complete cartilage defect area, were then embedded in paraffin and sectioned into a series of 4 μ m slices for subsequent staining.

H&E staining: The sections were dewaxed to water and placed in a high-definition constant staining pre-treatment solution for 1 min, followed by staining with hematoxylin solution for 3–5 min. After rinsing with tap water, hematoxylin differentiation solution was applied, followed by another rinse with tap water and then treat the sections with hematoxylin bluing solution, the sections were washed with running water. The sections were dehydrated in 95 % ethanol for 1 min, followed by staining with eosindye for 15 s. Finally, the sections were dehydrated, sealed, and images were captured and analyzed under a Nikon E100 bright-field microscope (Nikon, Japan).

Safranin O/fast green staining: After the above steps up to the dewaxing to water step, the sections stained in fast green dye solution for 1–5 min, excess dye solution was rinsed off with water until the cartilage was colorless, and soaked in 1 % hydrochloric acid and alcohol for 10 s, followed by a brief rinse with tap water. The sections were stained in safranin dye solution for 1–5 s, and then dehydrated rapidly in absolute ethanol for 5, 2, and 10 s, respectively, and then treated with xylene to transparent for 5 min. After being sealed with neutral gum, images were captured and analyzed under a Nikon E100 bright-field microscope (Nikon, Japan).

Immunohistochemical staining: After the above steps up to the dewaxing to water step, the sections underwent antigen repair and were naturally cooled before being washed with PBS. The sections were then placed in 3 % hydrogen peroxide solution and incubated at room temperature in the dark for 25 min, followed by washing with PBS. Next, the sections were covered with 3 % BSA solution to block non-specific binding and incubated at room temperature for 30 min. The excess blocking solution was gently shaken off, and the sections were placed flat in a wet box, then incubated overnight at 4 °C with the appropriately prepared primary antibody. After washing with PBS, the sections were covered with horseradish peroxidase-conjugated secondary antibody at room temperature and incubated for 50 min. Following PBS washing, freshly prepared DAB color development solution was added, and the sections were rinsed with tap water to terminate the color development. Subsequently, the sections were briefly stained with hematoxylin for approximately 3 min and rinsed with tap water, hematoxylin

differentiation solution for a few seconds, rinse with tap water, hematoxylin return to blue solution, and rinse with running water. Finally, the sections were dehydrated, sealed, and observed under a Nikon E100 bright-field microscope (Nikon, Japan) to analyze the staining results.

4.6.6. In vivo degradation experiment

Add RBITC solution to the SF solution to obtain a SF solution with an RBITC concentration of approximately 5 ppm. Then use this solution to prepare the corresponding SF scaffold. Implant the scaffold into the subcutaneous tissue of rats for degradation experiments. At specified time points (week 4 and week 8), retrieve the degraded scaffolds with/without coating from the subcutaneous tissue (3 replicate samples per group). Fix them in 4 wt% PFA solution for 48 h, followed by dehydration, paraffin embedding, and consecutive sectioning with a thickness of 4 μ m. Dry and dewax the paraffinized tissue sections, then stain them with DAPI staining solution. Capture images using a LSM 980 CLSM (Zeiss, Germany), and measure and analyze the fluorescence area of RBITC.

4.7. Statistical analysis

All data are shown as mean \pm SD. Sample size (n) for each statistical analysis was 3–5. The Shapiro–Wilk test was performed to evaluate the normality of the analyzed data. Statistical comparisons were conducted using two-tailed t-tests (two groups) and one-way ANOVA (three groups and above), followed by Tukey's post-test. $P < 0.05$ was considered to indicate statistical significance (* $p < 0.05$, ** $p < 0.01$, and *** $p < 0.001$). All statistical analyses were performed using GraphPad Prism 9.0 (GraphPad Software Inc., USA).

CRediT authorship contribution statement

Menglin Xiao: Writing – original draft, Formal analysis, Data curation. **Liangyan Sun:** Formal analysis, Data curation. **Kang Wu:** Formal analysis, Data curation. **Yuqi Ding:** Data curation. **Peipei Wang:** Data curation. **Chuangchuang Mu:** Data curation. **Jinrong Yao:** Project administration, Investigation. **Zhengzhong Shao:** Project administration, Investigation. **Bingjiao Zhao:** Writing – review & editing, Supervision, Resources, Project administration, Methodology, Funding acquisition, Conceptualization. **Xin Chen:** Writing – review & editing, Supervision, Resources, Project administration, Methodology, Funding acquisition, Conceptualization.

Ethics approval and consent to participate

All animal experiments were conducted following the ethical guidelines approved by the Ethics Committee of the Laboratory Animal Science Department of Fudan University (Approval No.202310039S).

Declaration of competing interest

The authors declare that they have no known competing financial interests or personal relationships that could have appeared to influence the work reported in this paper.

Appendix A. Supplementary data

Supplementary data to this article can be found online at <https://doi.org/10.1016/j.bioactmat.2025.03.005>.

References

- [1] E.R. Vina, C.K. Kwok, Epidemiology of osteoarthritis: literature update, *Curr. Opin. Rheumatol.* 30 (2018) 160–167.
- [2] E.A. Makris, A.H. Gomoll, K.N. Malizos, J.C. Hu, Repair and tissue engineering techniques for articular cartilage, *Nat. Rev. Rheumatol.* 11 (2015) 21–34.

- [3] C. Qi, J. Liu, Y. Jin, L. Xu, G. Wang, Z. Wang, L. Wang, Photo-crosslinkable, injectable sericin hydrogel as 3D biomimetic extracellular matrix for minimally invasive repairing cartilage, *Biomaterials* 163 (2018) 89–104.
- [4] D.J. Huey, J.C. Hu, K.A. Athanasiou, Unlike bone, cartilage regeneration remains elusive, *Science* 338 (2012) 917–921.
- [5] B.J. Huang, J.C. Hu, K.A. Athanasiou, Cell-based tissue engineering strategies used in the clinical repair of articular cartilage, *Biomaterials* 98 (2016) 1–22.
- [6] M. Li, Y. Jiang, Q. Hou, Y. Zhao, L. Zhong, X. Fu, Potential pre-activation strategies for improving therapeutic efficacy of mesenchymal stem cells: current status and future prospects, *Stem Cell Res. Ther.* 13 (2022) 146.
- [7] F.M. Chen, L.A. Wu, M. Zhang, R. Zhang, H.H. Sun, Homing of endogenous stem/progenitor cells for in situ tissue regeneration: promises, strategies, and translational perspectives, *Biomaterials* 32 (2011) 3189–3209.
- [8] Y. Yin, X. Li, X.T. He, R.X. Wu, H.H. Sun, F.M. Chen, Leveraging stem cell homing for therapeutic regeneration, *J. Dent. Res.* 96 (2017) 601–609.
- [9] J.R. Steadman, W.G. Rodkey, J.J. Rodrigo, Microfracture: surgical technique and rehabilitation to treat chondral defects, *Clin. Orthop. Relat. Res.* 391 (2001) S362–S369.
- [10] B.J. Cole, C. Pascual-Garrido, R.C. Grumet, Surgical management of articular cartilage defects in the knee, *Instr. Course Lect.* 59 (2010) 181–204.
- [11] B. Chukpauwong, E.M. Berkson, G.H. Theodore, Microfracture for osteochondral lesions of the ankle: outcome analysis and outcome predictors of 105 cases, *Arthroscopy* 24 (2008) 106–112.
- [12] J. Lu, X. Shen, X. Sun, H. Yin, S. Yang, C. Lu, Y. Wang, Y. Liu, Y. Huang, Z. Yang, X. Dong, C. Wang, Q. Guo, L. Zhao, X. Sun, S. Lu, A.G. Mikos, J. Peng, X. Wang, Increased recruitment of endogenous stem cells and chondrogenic differentiation by a composite scaffold containing bone marrow homing peptide for cartilage regeneration, *Theranostics* 8 (2018) 5039–5058.
- [13] K.B. Lee, V.T. Wang, Y.H. Chan, J.H. Hui, A novel, minimally-invasive technique of cartilage repair in the human knee using arthroscopic microfracture and injections of mesenchymal stem cells and hyaluronic acid—a prospective comparative study on safety and short-term efficacy, *Ann. Acad. Med. Singapore* 41 (2012) 511–517.
- [14] A. Gobbi, G. Karnatzikos, A. Kumar, Long-term results after microfracture treatment for full-thickness knee chondral lesions in athletes, *Knee Surg. Sports Traumatol. Arthrosc.* 22 (2014) 1986–1996.
- [15] M. Asik, F. Ciftci, C. Sen, M. Erdil, A. Atalar, The microfracture technique for the treatment of full-thickness articular cartilage lesions of the knee: midterm results, *Arthroscopy* 24 (2008) 1214–1220.
- [16] S. Pacelli, S. Basu, J. Whitlow, A. Chakravarti, F. Acosta, A. Varshney, S. Modaresi, C. Berkland, A. Paul, Strategies to develop endogenous stem cell-recruiting bioactive materials for tissue repair and regeneration, *Adv. Drug Deliv. Rev.* 120 (2017) 50–70.
- [17] W. Zhang, H. Ouyang, C.R. Dass, J. Xu, Current research on pharmacologic and regenerative therapies for osteoarthritis, *Bone Res.* 4 (2016) 15040.
- [18] H. Xuan, H. Hu, C. Geng, J. Song, Y. Shen, D. Lei, Q. Guan, S. Zhao, Z. You, Biofunctionalized chondrogenic shape-memory ternary scaffolds for efficient cell-free cartilage regeneration, *Acta Biomater.* 105 (2020) 97–110.
- [19] Y. Luo, M. Xiao, B.S. Almaqami, H. Kang, Z. Shao, X. Chen, Y. Zhang, Regenerated silk fibroin based on small aperture scaffolds and marginal sealing hydrogel for osteochondral defect repair, *Biomater. Res.* 27 (2023) 50.
- [20] B. Kundu, R. Rajkhowa, S.C. Kundu, X. Wang, Silk fibroin biomaterials for tissue regenerations, *Adv. Drug Deliv. Rev.* 65 (2013) 457–470.
- [21] W. Huang, S. Ling, C. Li, F.G. Omenetto, D.L. Kaplan, Silkworm silk-based materials and devices generated using bio-nanotechnology, *Chem. Soc. Rev.* 47 (2018) 6486–6504.
- [22] M. Xiao, J. Yao, Z. Shao, X. Chen, Silk-based 3D porous scaffolds for tissue engineering, *ACS Biomater. Sci. Eng.* 10 (2024) 2827–2840.
- [23] X. Wang, E. Wenk, X. Zhang, L. Meine, G. Vunjak-Novakovic, D.L. Kaplan, Growth factor gradients via microsphere delivery in biopolymer scaffolds for osteochondral tissue engineering, *J. Contr. Release* 134 (2009) 81–90.
- [24] X. Wang, T. Yucel, Q. Lu, X. Hu, D.L. Kaplan, Silk nanospheres and microspheres from silk/PVA blend films for drug delivery, *Biomaterials* 31 (2010) 1025–1035.
- [25] G.S. Nowakowski, M.S. Dooner, H.M. Valinski, A.M. Mihaliak, P.J. Quesenberry, P. S. Becker, A specific heptapeptide from a phage display peptide library homes to bone marrow and binds to primitive hematopoietic stem cells, *Stem Cell.* 22 (2004) 1030–1038.
- [26] X. Sun, H. Yin, Y. Wang, J. Lu, X. Shen, C. Lu, H. Tang, H. Meng, S. Yang, W. Yu, Y. Zhu, Q. Guo, A. Wang, W. Xu, S. Liu, S. Lu, X. Wang, J. Peng, In situ articular cartilage regeneration through endogenous reparative cell homing using a functional bone marrow-specific scaffolding system, *ACS Appl. Mater. Interfaces* 10 (2018) 38715–38728.
- [27] B. Huang, P. Li, M. Chen, L. Peng, X. Luo, G. Tian, H. Wang, L. Wu, Q. Tian, H. Li, Y. Yang, S. Jiang, Z. Yang, K. Zha, X. Sui, S. Liu, Q. Guo, Hydrogel composite scaffolds achieve recruitment and chondrogenesis in cartilage tissue engineering applications, *J. Nanobiotechnol.* 20 (2022) 25.
- [28] F.Y. Cao, W.N. Yin, J.X. Fan, R.X. Zhuo, X.Z. Zhang, A novel function of BMHP1 and cBMHP1 peptides to induce the osteogenic differentiation of mesenchymal stem cells, *Biomater. Sci.* 3 (2015) 345–351.
- [29] Y. Ono, S. Ishizuka, C.B. Knudson, W. Knudson, Chondroprotective effect of kartogenin on CD44-mediated functions in articular cartilage and chondrocytes, *Cartilage* 5 (2014) 172–180.
- [30] B. Luo, S. Wang, X. Song, S. Chen, Q. Qi, W. Chen, X. Deng, Y. Ni, C. Chu, G. Zhou, X. Qin, D. Lei, Z. You, An encapsulation-free and hierarchical porous triboelectric scaffold with dynamic hydrophilicity for efficient cartilage regeneration, *Adv. Mater.* 36 (2024) e2401009.
- [31] K. Johnson, S. Zhu, M.S. Tremblay, J.N. Payette, J. Wang, L.C. Bouchez, S. Meeusen, A. Althage, C.Y. Cho, X. Wu, P.G. Schultz, A stem cell-based approach to cartilage repair, *Science* 336 (2012) 717–721.
- [32] G. Liu, Q. Guo, C. Liu, J. Bai, H. Wang, J. Li, D. Liu, Q. Yu, J. Shi, C. Liu, C. Zhu, B. Li, H. Zhang, Cytomodulin-10 modified GelMA hydrogel with kartogenin for in-situ osteochondral regeneration, *Acta Biomater.* 169 (2023) 317–333.
- [33] J. Xu, Q. Feng, Q. S. Lin, W. Yuan, R. Li, J. Li, K. Wei, X. Chen, K. Zhang, Y. Yang, T. Wu, B. Wang, M. Zhu, R. Guo, G. Li, L. Bian, Injectable stem cell-laden supramolecular hydrogels enhance in situ osteochondral regeneration via the sustained co-delivery of hydrophilic and hydrophobic chondrogenic molecules, *Biomaterials* 210 (2019) 51–61.
- [34] V.R. Sinha, A. Trehan, Biodegradable microspheres for protein delivery, *J. Contr. Release* 90 (2003) 261–280.
- [35] Y. Liu, G. Dziditor, T.T. Le, T. Vinikoor, K. Morgan, E.J. Curry, R. Das, A. McClinton, E. Eisenberg, L.N. Apuzzo, K.T.M. Tran, P. Prasad, T.J. Flanagan, S. W. Lee, H.M. Kan, M.T. Chorsi, K.W.H. Lo, C.T. Laurencin, T.D. Nguyen, Exercise-induced piezoelectric stimulation for cartilage regeneration in rabbits, *Sci. Transl. Med.* 14 (2022) eabi7282.
- [36] Y. Chen, T. Wu, S. Huang, C.W. Suen, X. Cheng, J. Li, H. Hou, G. She, H. Zhang, H. Wang, X. Zheng, Z. Zha, Sustained release SDF-1 α /TGF- β 1-loaded silk fibroin-porous gelatin scaffold promotes cartilage repair, *ACS Appl. Mater. Interfaces* 11 (2019) 14608–14618.
- [37] W. Zhang, C. Ling, A. Zhang, H. Liu, Y. Jiang, X. Li, R. Sheng, Q. Yao, J. Chen, An all-silk-derived functional nanosphere matrix for sequential biomolecule delivery and in situ osteochondral regeneration, *Bioact. Mater.* 5 (2020) 832–843.
- [38] Z. Mao, X. Bi, C. Wu, Y. Zheng, X. Shu, S. Wu, J. Guan, R.O. Ritchie, A cell-free silk fibroin biomaterial strategy promotes in situ cartilage regeneration via Programmed releases of bioactive molecules, *Adv. Healthcare Mater.* 12 (2023) 2201588.
- [39] X. Dong, C. Li, M. Zhang, Y. Zhao, Z. Zhao, W. Li, X. Zhang, Multifunctional injectable hydrogel for effective promotion of cartilage regeneration and protection against osteoarthritis: combined chondroinductive, antioxidative and anti-inflammatory strategy, *Sci. Technol. Adv. Mater.* 23 (2022) 361–375.
- [40] L. Chen, Z. Ni, J. Huang, R. Zhang, J. Zhang, B. Zhang, L. Kuang, X. Sun, D. Zhang, N. Su, H. Qi, J. Yang, M. Jin, F. Luo, H. Chen, S. Zhou, X. Du, J. Ouyang, Z. Wang, Y. Xie, Q. Tan, L. Chen L, Long term usage of dexamethasone accelerating accelerates the initiation of osteoarthritis via enhancing chondrocyte apoptosis and the extracellular matrix calcification and apoptosis of chondrocytes, *Int. J. Biol. Sci.* 17 (2021) 4140–4153.
- [41] M. McGill, J.M. Coburn, B.P. Partlow, X. Mu, D.L. Kaplan, Molecular and macro-scale analysis of enzyme-crosslinked silk hydrogels for rational biomaterial design, *Acta Biomater.* 63 (2017) 76–84.
- [42] V.P. Ribeiro, S. Pina, J.B. Costa, I.F. Cengiz, L. García-Fernández, M.D. M. Fernández-Gutiérrez, O.C. Paiva, A.L. Oliveira, J. San-Román, J.M. Oliveira, R. L. Reis, Enzymatically cross-linked silk fibroin-based hierarchical scaffolds for osteochondral regeneration, *ACS Appl. Mater. Interfaces* 11 (2019) 3781–3799.
- [43] L. Zhang, P. Yang, R. Guo, J. Sun, R. Xie, W. Yang, Molecular and macro-scale analysis of enzyme-crosslinked silk hydrogels for rational biomaterial design, *Acta Biomater.* 63 (2017) 76–84.
- [44] Y. Dong, Y. Liu, Y. Chen, X. Sun, L. Zhang, Z. Zhang, Y. Wang, C. Qi, S. Wang, Q. Yang, Spatiotemporal regulation of endogenous MSCs using a functional injectable hydrogel system for cartilage regeneration, *NPG Asia Mater.* 13 (2021) 71.
- [45] L. Chen, L. Sun, W. Liu, J. Yao, Z. Shao, B. Zhao, X. Chen, Long-lasting thixotropic natural polymeric hydrogel based on silk nanofibrils, *ACS Biomater. Sci. Eng.* 9 (2023) 4168–4177.
- [46] J. Wen, J. Yao, X. Chen, Z. Shao, Silk fibroin acts as a self-emulsifier to prepare hierarchically porous silk fibroin scaffolds through emulsion-ice dual templates, *ACS Omega* 3 (2018) 3396–3405.
- [47] W. Lu, L. Sun, J. Yao, B. Zhao, Y. Liu, Z. Shao, X. Chen, Protein-inorganic hybrid porous scaffolds for bone tissue engineering, *J. Mater. Chem. B* 10 (2022) 6546–6556.
- [48] L. Sun, M. Xiao, L. Chen, L. Ni, X. Chen, L. Zhang, J. Yao, Z. Shao, B. Zhao, X. Chen, Y. Liu, Enhanced tissue regeneration through immunomodulatory extracellular vesicles encapsulated in diversified silk-based injectable hydrogels, *Adv. Healthcare Mater.* (2024) 2401460.